

1 **Landscape response to tectonic deformation and cyclic climate change since ca. 800 ka**
2 **in the southern Central Andes**

3
4 Elizabeth N. Orr^{1,2*}, Taylor F. Schildgen^{1,3}, Stefanie Tofelde⁴, Hella Wittmann¹ and Ricardo N.
5 Alonso⁵

6
7 1: GFZ German Research Centre for Geosciences, Telegrafenberg, 14473 Potsdam, Germany

8 2: Department of Geography, Durham University, Durham, DH1 3LE, United Kingdom

9 3: Institute for Geosciences, University of Potsdam, Karl-Liebknecht-Str. 24-25, 14476 Potsdam, Germany

10 4: Institute of Geological Sciences, Freie Universität Berlin, 12249 Berlin, Germany

11 5: Facultad de Ciencias Naturales, Universidad Nacional de Salta, Salta, 4400 Argentina

12 *Corresponding author: Elizabeth N. Orr (elizabeth.orr2@durham.ac.uk)

13
14 **Abstract**

15 Theory suggests that the response time of alluvial channel long-profiles to perturbations in climate is
16 related to the magnitude of the forcing and the length of the system. Shorter systems may record a
17 higher frequency of forcing compared to longer systems. Empirical field evidence that system length
18 plays a role in the climate periodicity preserved within the sedimentary record is, however, sparse. The
19 Toro Basin in the Eastern Cordillera of NW Argentina provides an opportunity to test these theoretical
20 relationships as this single source-to-sink system contains a range of sediment deposits, located at
21 varying distances from the source. A suite of eight alluvial fan deposits is preserved along the western
22 flanks of the Sierra de Pascha. Farther downstream, a flight of cut-and-fill terraces have been linked to
23 eccentricity-driven (100-kyr) climate cycles since ca. 500 ka. We applied cosmogenic radionuclide
24 (¹⁰Be) exposure dating to the fan surfaces to explore (1) how channel responses to external perturbations
25 may or may not propagate downstream, and (2) the differences in landscape response to forcing
26 frequency as a function of channel length. We identified two generations of fan surfaces: the first (G1)
27 records surface activity and abandonment between ca. 800 and 500 ka and the second (G2) within the
28 last 100 kyr. G1 fans record a prolonged phase of net incision, which has been recognised throughout
29 the Central Andes, and was likely triggered by enhanced 100-kyr global glacial cycles following the
30 Mid-Pleistocene Transition. Relative fan surface stability followed, while 100-kyr cut-and-fill cycles
31 occurred downstream, suggesting a disconnect in behaviour between the two channel reaches. G2 fans
32 record higher frequency climate forcing, possibly the result of precessional forcing of climate (ca.
33 21/40-kyr timescales). The lack of a high-frequency signal farther downstream provides field support
34 for theoretical predictions of a filtering of high-frequency climate forcing with increasing channel
35 length. We show that multiple climate periodicities can be preserved within the sedimentary record of
36 a single basin. Differences in the timing of alluvial fan and fluvial terrace development in the Toro
37 Basin appear to be associated with how channel length affects fluvial response times to climate forcing
38 as well as local controls on net incision, such as tectonic deformation.

Deleted: s

40 **Plain Language Summary**

41 Fluvial terraces and alluvial fans in the Toro Basin, NW Argentina record river evolution and global
42 climate cycles over time. Landform dating reveals lower-frequency climate cycles (100-kyr) preserved
43 downstream and higher-frequency cycles (21/40-kyr) upstream, supporting theoretical predications that
44 longer rivers filter out higher-frequency climate signals. This finding improves our understanding of
45 the spatial distribution of sedimentary paleoclimate records within landscapes.

46

47

48 **1. Introduction**

49

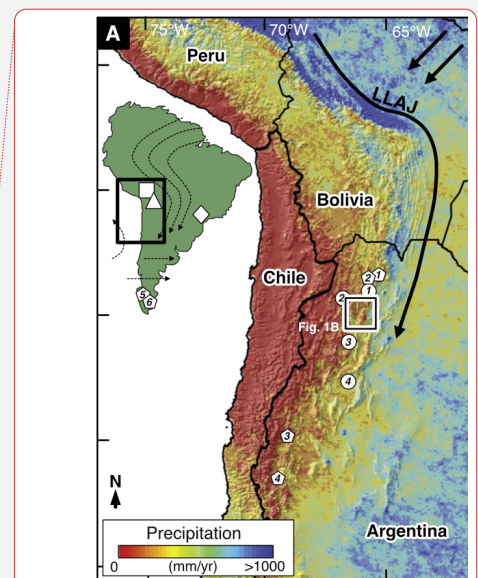
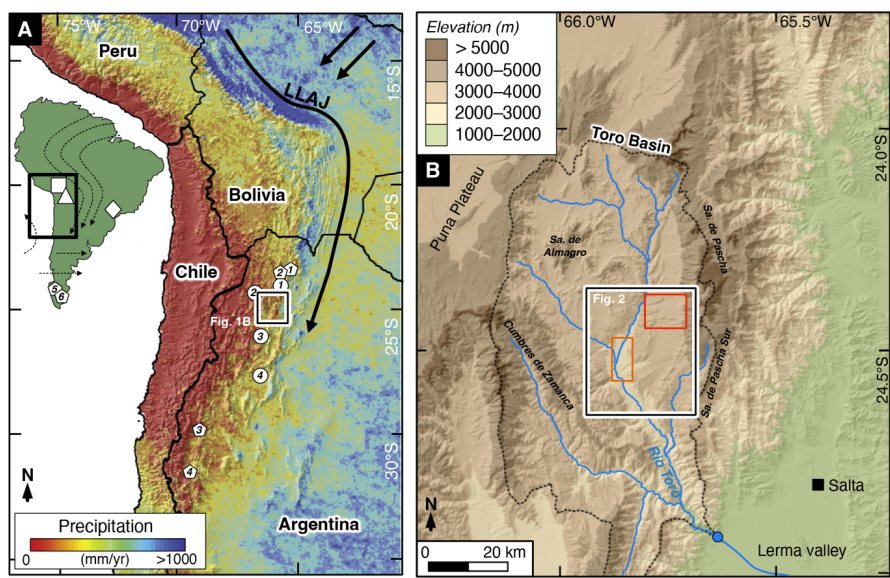
50 Fluvial landforms, sediment deposits and the channel form of alluvial systems can be used to reveal
51 landscape response to past environmental change (Castelltort and Van Den Driessche, 2003, Godard et
52 al., 2013; Dey et al., 2016; Romans et al., 2016; Mescolotti et al., 2021). Alluvial channels respond to
53 climate or tectonic driven changes in water discharge, sediment discharge, or base level elevation by
54 adjusting at least one of their characteristics: bed slope, channel width, channel depth, sediment
55 transport rates or grain-size distribution (Mackin 1948; Savi et al., 2020). We observe this channel
56 adjustment via sediment aggradation or incision events, which modify channel bed elevations (Howard,
57 1982; van den Berg et al., 2008; Wickert and Schildgen, 2019; Tofelde et al., 2019). Fluvial landforms
58 such as terraces and alluvial fans, which develop along these channels because of this aggradation or
59 incision, can provide a useful record of how the alluvial-channel system has evolved over time (Rohais
60 et al., 2012; Armitage et al., 2013; Kober et al., 2013; Counts et al., 2015; Mather et al., 2017; Tofelde
61 et al., 2021).

62

63 Theory suggests that the time required for an alluvial-channel long profile to adjust to a change in
64 climate forcing (response time) varies with the magnitude and type of the forcing (sediment supply
65 versus water supply) and the length of the system; shorter systems respond faster and, hence, may record
66 a higher frequency of forcing compared to longer systems (Paola et al., 1992; Castelltort and Van Den
67 Driessche, 2003; Godard et al., 2013; McNab et al., 2023). The length scale over which periodic forcing
68 delivered at the channel head affects the channel long profile is proportional to the square root of the
69 period of the forcing (Paola et al., 1992), which means that higher frequency forcing is filtered out with
70 distance downstream. Evidence of this relationship is preserved in several sedimentary basins in the
71 Central Andes. Tributary catchments of the Humahuaca Basin (23°S) retain late Quaternary fluvial
72 deposits between 10 and 100 km downstream from the basin headwaters, which record precessional (21
73 kyr) cycles in aggradation and incision (Schildgen et al., 2016). In the Toro Basin (24.5°S), a flight of
74 fluvial cut-and-fill terraces with periodicity of 100-kyr has been linked to eccentricity-driven climate
75 change (Tofelde et al., 2017). These terraces have an upstream channel length of ~60–80 km. Pliocene-

Deleted: can

77 Late Pleistocene sediment deposits are preserved ~140–160 km downstream from the headwaters of
 78 the Iruya Basin (22°S) of the northern Central Andes and record long eccentricity (400-kyr) cycles
 79 (Fisher et al., 2023). Crucially, only a single climate periodicity has been recorded in each these basins
 80 to date. To further test this theoretical relationship between climate periodicity and system length, we
 81 aim to investigate whether multiple periodicities can be preserved within a single basin, and if this is
 82 the case, whether higher frequency climate forcing is only observed in the uppermost reaches of the
 83 basin.
 84



85
 86 **Figure 1.** Overview of the topography, rainfall and moisture transport of the Central Andes. A) TRMM2B31 ([Tropical Rainfall](#)
 87 [Measuring Mission](#)) rainfall map (Bookhagen and Strecker, 2008). Moisture is transported (black arrows) from Atlantic
 88 sources during the SASM ([South American Summer Monsoon](#)) by the Low-Level Andean Jet (LLAJ; Vera et al., 2006). The
 89 Toro Basin is outlined by the white-black bordered box. Circle symbols denote regional glacial record locations: (1) Nevado
 90 de Chañi (24.0°S, 65.7°W; Martini et al., 2017), (2) Quevar Volcano (24.4°S, 66.8°W; Luna et al., 2018), (3) Sierra de Quilmes
 91 (26.2°S, 66.2°W; Zech et al., 2017) and the (4) Sierra de Aconquija (27.2°S, 66.1°W; D'Arcy et al., 2019a). Pentagon symbols
 92 denote [Mid Pleistocene Transition](#) (MPT) geomorphic record locations: (1) Casa Grande Basin (23°S, 66.5°W; Pingel et al.,
 93 2019b), (2) Salinas Grandes Basin (23.5°S, 66°W; Pingel et al., 2019b), (3) Iglesia Basin (30.5°S, 69°W; Terrizzano et al.,
 94 2017), (4) Calingasta Basin (32°S, 69.5°W; Peri et al., 2022), (5) Rio Deseado (47°S, 72°W; Tobal et al., 2021), (6) Rio Santa
 95 Cruz (50°S, 73°W; Milanez Fernandes, 2023). Inset map of South America indicates Fig. 1A extent and the location of the
 96 Lake Titicaca (square symbol; Fritz et al., 2007), Salar de Uyuni (triangle symbol; Baker et al., 2001) and Botuverá Cave
 97 (diamond symbol; Wang et al., 2007) paleoenvironmental records. Dashed arrows outline the moisture-bearing low-level
 98 airflow patterns for South America which are deflected by the Andean topography. B) Topography of the Toro Basin (ca. 4000
 99 km², 1500–5900 m asl) from [12-m resolution](#) TanDEM-X ([10-m vertical resolution](#)) elevation data. Basin outlined by dashed
 100 black line. Upper basin delineated by white-black bordered rectangle (see Fig. 2). Toro alluvial fans and fluvial terraces
 101 outlined by red and orange rectangles, respectively. Basin outlet and start of long profile in Fig. 2 is shown by blue circle. Sa-
 102 - Sierra.
 103

Deleted: 2

104 Approximately 30 km upstream of the 100-kyr cut-and fill terraces in the Toro Basin is a suite of well-
 105 preserved alluvial fan surfaces which extend from tributary catchments that drain the Sierra de Pascha
 106 (Fig. 1). There is limited evidence of sediment storage in these tributary catchments en route to the fans.

109 With an upstream channel length of ~10 km, this fan record may capture geomorphic change linked to
110 a higher frequency climate forcing than the downstream terraces. The Toro Basin alluvial-channel
111 system therefore allows us to explore (1) how channel responses to external perturbations may or may
112 not propagate downstream, and (2) the differences in landscape response to forcing frequency as a
113 function of channel length when comparing the upper basin alluvial fan deposits with the lower basin
114 terrace sequence.

115

116 To address these aims, we dated the suite of fan surfaces in the upper Toro Basin using *in situ*-¹⁰Be
117 cosmogenic radionuclide (CRN) dating. We used our new Toro fan chronostratigraphy in conjunction
118 with the fluvial terrace record of Tofelde et al. (2017) to further characterise the evolution of the Toro
119 Basin over the last million years.

120

121 2. Regional setting

122

123 The Toro Basin (24.5°S) is an intermontane basin in the Eastern Cordillera of NW Argentina, located
124 between the high elevation Puna Plateau to the west and the low elevation Andean foreland to the east
125 (Fig. 1). The mainly gravel-bedded Río Toro flows predominantly south from the low relief upper
126 reaches of the basin with thick successions of preserved sediment, which are the focus of this study
127 (referred to as the upper Toro Basin herein), through a steep bedrock gorge, before draining into the
128 Cabra Corral reservoir in the Lerma valley (Marrett and Strecker 2000). The diffuse shifts in channel
129 steepness along its course are characteristic of arid, tectonically active landscapes with mechanically
130 strong basement rocks (Fig. 2B, C) (Bernard et al., 2019, Zondervan et al., 2020; Seagren and
131 Schoenbohm, 2021).

132

133 2.1 Geology and tectonic setting

134 The upper Toro Basin is confined by three reverse-fault bounded basement ranges: 1) the Cumbres de
135 Zamaca bounded by the west-dipping Solá Fault in the west, 2) the Sierra de Almagro bounded by the
136 northwest-dipping San Bernardo fault in the north, and 3) the Sierra de Pascha Ranges and the east-
137 dipping Gólgota Fault in the east (Alonso 1992; Marrett and Strecker 2000) (Fig. 1, 2). The Solá fault
138 has been active since at least the Late Miocene, and tectonic deformation from the Miocene to mid-
139 Pleistocene has been recorded along the San Bernardo and Gólgota faults (Marrett and Strecker 2000;
140 DeCelles et al., 2011; Pearson et al., 2013; Pingel et al., 2020). The Gólgota fault reactivated after ca.
141 0.98 Ma (Hilley and Strecker 2005).

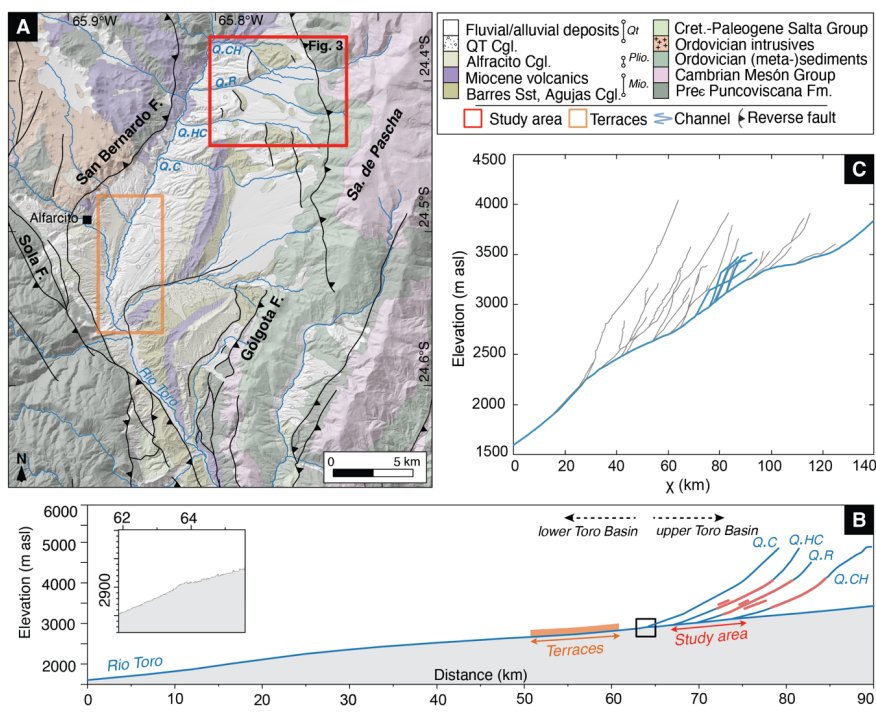
142

143 This study focuses on a suite of fans that emerge from the tributary catchments of the Sierra de Pascha
144 and are located ~30 km upstream from the cut-and-fill terraces recording 100-kyr climate cyclicity
145 described by Tofelde et al. (2017). The Pascha Ranges are characterised by meta-sediments of the Late

Deleted: ; DeCelles et al., 2011

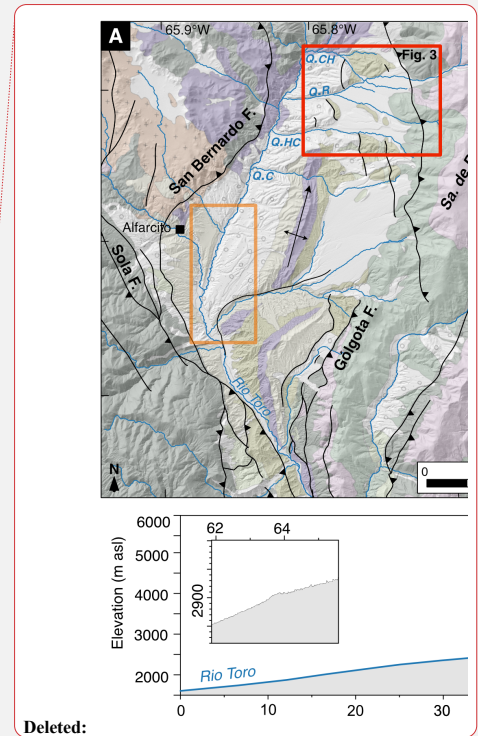
Deleted: Pliocene

148 Proterozoic-Cambrian Puncoviscana Formation and quartzites and shales of the Cambrian Mesón
 149 Group (Schwab and Schafer 1976; García et al., 2013). Long term rock-uplift rates based on structural
 150 reconstructions range between 0.4 and 0.6 mm/yr (Hilley and Strecker 2005).
 151



152
 153 **Figure 2.** Geology and topography of the upper Toro Basin. A) Geologic map with the alluvial fan sequence location (our
 154 study area, Fig. 3) and cut-and-fill terraces described by Tofelde et al. (2017) outlined by red and orange rectangles
 155 respectively. Other terraces extend discontinuously along the basin's channel length but remain undated. Map adapted from
 156 Segemar 250k geological maps and Pingel et al. (2020). Abbreviations: Sa. – Sierra, F – Fault, Q.CH – Quebrada (mountain
 157 stream) Chacra Huaico, Q.R – Quebrada Rosal, Q. HC – Quebrada Huasa Ciénaga, Q.C – Quebrada del Chorro, Q.Ca –
 158 Quebrada Carachi. **Fm – Formation, Cgl – Conglomerates, Sst – Sandstone.** B) Long profile of Toro Basin with tributary
 159 profiles of upper basin study area. Upper and lower basin reaches are indicated by dashed arrows. Full basin profile extracted
 160 from fluvial network outlined in Fig. 1. Alluvial fan and terrace surfaces are projected onto profiles. Inset: Higher resolution
 161 plot of proposed knickzone at confluence between the Río Toro and Quebrada del Chorro (outlined in main plot by black box).
 162 C) Chi-plot of all channels with a minimum drainage area of 1 km² within the Toro basin using a reference concavity index of
 163 0.45. Bold lines highlight the main river channel and tributary catchments within our study area.
 164

165 The Middle Miocene Barres Sandstone and Agujas Conglomerates, interbedded with lava flows, and
 166 the Pliocene-Pleistocene Alfarcito Conglomerates, make up the west-tilted strata, which lay between the
 167 fan deposits and the Río Toro (Fig. 2A; Hilley and Strecker, 2005; Mazzuoli et al., 2008). Resistant
 168 Barres, Agujas and Alfarcito units characterise several erosional surfaces that stand ~700 m above the
 169 modern river channel. Incision into these tectonically deformed units by tributaries draining the Sierra
 170 de Pascha is thought to have occurred after 0.98 Ma (Hilley and Strecker, 2005), the age of an



Deleted:
 Deleted:
 Deleted: are exposed along a north-trending anticline
 Deleted: ies
 Deleted: ; DeCelles et al., 2011; Robledo et al., 2020

177 intercalated ash unit dated from the uppermost layers of the Alfarcito Conglomerate (Marrett et al.,
178 1994). Undeformed Quaternary conglomerates (also called ‘Terrace Conglomerates’) and
179 fluvial/alluvial deposits either mantle or infill this tectonically deformed and eroded palaeotopography
180 (Fig. 2; Marrett and Strecker, 2000; Hilley and Strecker, 2005). The Río Toro sets the local base level
181 for the Pascha tributaries today (Tofelde et al., 2017).

182

183 2.2 Climatic setting

184 Moisture mainly governed by the South American Summer Monsoon (SASM) system is directed by the
185 Low Level Andean Jet (LLAJ) from the Atlantic Ocean and Amazon Basin to the Central Andes (Vera
186 et al., 2006; Alonso et al., 2006; Bookhagen and Strecker 2008; Castino et al., 2017). The semi-arid
187 Toro Basin is located towards the southern limit of this moisture conveyor and receives rainfall that
188 ranges from ~900 mm/yr at the outlet to < 200 mm/yr in the basin headwaters (Fig. 1; Bookhagen and
189 Strecker 2008). The Sierra de Pascha acts as an orographic barrier, causing the eastern flanks of the
190 range to be comparatively wetter than the basin interior. The intensity of the SASM and resultant
191 moisture supply to the Central Andes has been variable over time (see Baker and Fritz, 2015 for detailed
192 review). Paleoenvironmental records from Argentina, Chile and Bolivia show that SASM precipitation
193 has varied with changes in insolation over 19 to 25-kyr (precession) (Godfrey et al., 2003, Fritz et al.,
194 2004, 2010; Placzek et al., 2006; Bobst et al., 2001) and 100-kyr (eccentricity) (Fritz et al., 2007;
195 Gosling et al., 2008) cycles. The Central Andes are also subject to increased rainfall during periods of
196 northern hemispheric cooling, whereby the Atlantic part of the intertropical convergence zone (ITCZ)
197 is forced southward, bringing moisture with it (Broccoli et al., 2006; Mosblech et al., 2012; Novello
198 et al., 2017; Crivellari et al., 2018). These cold and wet conditions correlate with phases of glacial advance
199 and rising lake levels (Haselton et al., 2002; Vizy and Cook, 2007; Martin et al., 2018; Mey et al., 2020).

200

201 Successions of glacial moraines are preserved within the Sierra de Pascha tributary catchments and are
202 indicative of repeated late Quaternary glaciations (Tofelde et al., 2018). Glacial records proximal to the
203 Toro Basin (24-27.2°S) underline the sensitivity of Andean glaciers to SASM precipitation intensity
204 and temperature (Martini et al., 2017; Zech et al., 2017; Luna et al., 2018; D’Arcy et al., 2019a; Mey
205 et al., 2020). The timing of regional glacial stages is invariably in phase with insolation cycles, periods of
206 SASM strengthening and/or northern hemispheric events (e.g., Younger Dryas, Last Glacial Maximum)
207 (D’Arcy et al., 2019a).

208

209 2.3 Basin sediment infilling and incision

210 Thick successions of sediment, together with subtle knickzones and hairpin turns in the Río Toro reflect
211 a complex late Cenozoic history of basin filling and evacuation (Strecker et al., 2009; Hain et al., 2011;
212 Vezzoli et al., 2012; Pingel et al., 2020), base level perturbations and tectonic deformation (Marrett and
213 Strecker, 2000; Hilley and Strecker, 2005; Tofelde et al., 2017), and drainage reorganization (Seagren

Deleted: South American low-level jet

Deleted: (SALLJ)

216 and Schoenbohm, 2021; Seagren et al., 2022). Given our interest in the Quaternary deposits of the upper
217 Toro Basin, we focus our attention on how the basin has evolved over the last one million years.

218

219 After deposition of the Alfarcito conglomerates concluded at ca. 0.98 Ma, the Toro Basin was evacuated
220 to a base level lower than today (Hilley and Strecker, 2005). Renewed hydrological connectivity
221 between the Toro Basin and the Lerma Valley likely caused widespread basin sediment evacuation and
222 incision of the (paleo)topography. Uplift of the Sierra de Pascha Sur also recommenced sometime after
223 ca. 0.98 Ma (Hilley and Strecker, 2005). The newly uplifted range impeded the delivery of precipitation
224 to the basin interior, and by ca. 0.8 Ma, the semi-arid conditions of today were established (Kleinert and
225 Strecker 2001; Strecker et al. 2007; Pingel et al., 2020). The mechanically strong basement rocks, and
226 a potentially reduced sediment transport capacity, meant that incision was unable to keep pace with the
227 renewed rock uplift. This forced widespread aggradation and a decrease in relief upstream of the
228 Gólgota fault, and channel steepening within the bedrock gorge cutting through the Sierra de Pascha
229 Sur (Fig. 2; Hilley and Strecker, 2005; Strecker et al., 2009; García et al., 2013). External drainage
230 either became restricted or ceased at this time (Marrett et al. 1994; Hain et al., 2011; Pingel et al.,
231 2019a). Evidence for a similar sequence of events is seen in the Humahuaca, Casa Grande and
232 Calchaquí basins (23°S), where renewed range uplift reduced hydrological connectivity and caused
233 sediment infilling (Robinson et al., 2005; Hain et al., 2011; García et al., 2013; Pingel et al., 2013, 2016,
234 2019a; Streit et al., 2017; Seagren et al., 2022). Although there are some uncertainties about the exact
235 timing, connectivity between the Toro Basin and the foreland is thought to have been re-established due
236 to external base-level change (Seagren and Schoenbohm, 2021).

237

238 The Quaternary “Terrace Conglomerates” were deposited within the Toro Basin starting from ca. 0.94
239 Ma and are considered part of this phase of uplift-induced basin infilling (Hilley and Strecker, 2005). A
240 flight of six fluvial terrace levels in the lower basin are preserved between 20 and 200 m above the
241 modern Río Toro (Fig. 2). Cosmogenic exposure-age dating of terraces, burial dating of the sediments,
242 and zircon U-Pb ages of intercalated ashes from the terrace levels revealed multiple 100-kyr cut-and-
243 fill sedimentary cycles starting from ca. 500 ka (Tofelde et al., 2017). The phases of incision correspond
244 with cold, wet glacial periods, when sediment transport capacity apparently exceeded sediment flux,
245 whereas aggradation occurred when sediment transport was considerably reduced (Tofelde et al., 2017).
246 Moreover, the calculated net incision rate through the terrace sequence of 0.4 mm/yr from ca. 500 ka is
247 consistent with long term rock-uplift rates of the Sierra de Pascha Sur (Hilley and Strecker, 2005).
248 Tofelde et al. (2017) thus concluded that while the renewed uplift of the Sierra de Pascha Sur helped
249 initiate the deposition of the Terrace Conglomerates, the periodicity of the cut-and-fill cycles is best
250 explained by orbitally driven climate forcing, with net incision likely associated with the channel
251 response to ongoing rock-uplift. Today, catchment-averaged erosion rates for catchments draining the
252 Sierra de Pascha range between <0.03 and 0.12 mm/yr (Tofelde et al., 2018).

Deleted: at the basin outlet

254

255 3. Methodology

256

257 To evaluate past channel behaviour and landscape response to climate and/or tectonic forcing for the
258 upper Toro Basin, we applied CRN exposure dating to the suite of fan surfaces along the western front
259 of the Sierra de Pascha (Fig. 1, 2).

260

261 Alluvial fan CRN ages record the timing of active sediment deposition or surface stability between
262 periods of channel avulsion and incision (Dühnforth et al., 2007; D’Arcy et al., 2019b), which lead to
263 abandonment of the fan surface. This abandonment can occur due to changes in sediment supply
264 (Brooke et al., 2018; Tofelde et al., 2019), tectonic deformation and base level change (Ganev et al.,
265 2010; Mouslopoulou et al., 2017), climate-induced changes in water discharge (Steffen et al., 2010;
266 Savi et al., 2016) or drainage reorganization (Bufe et al., 2017). Because fan surfaces can remain active
267 for 10^2 – 10^5 years before being incised (Cesta and Ward, 2016; Dühnforth et al., 2017; Ratnayaka et al.,
268 2019; Peri et al., 2022), the age distribution or minimum exposure age of boulders on an alluvial fan
269 surface will not necessarily tightly constrain the timing of abandonment. Instead, the distribution of
270 CRN ages, after excluding clear outliers, more likely reflects phases of fan activity, and at best, provide
271 a minimum age limit for the onset of incision leading to eventual surface abandonment (D’Arcy et al.,
272 2019b).

273

274 We mapped the upper Toro Basin fans using TanDEM-X (12 m-resolution) data and Google Earth
275 imagery. The stratigraphic relationships among the different fan surfaces were used to inform the
276 cosmogenic radionuclide (CRN) sampling strategy (e.g., McFadden et al., 1989; Hughes et al., 2010;
277 Hedrick et al., 2013).

278

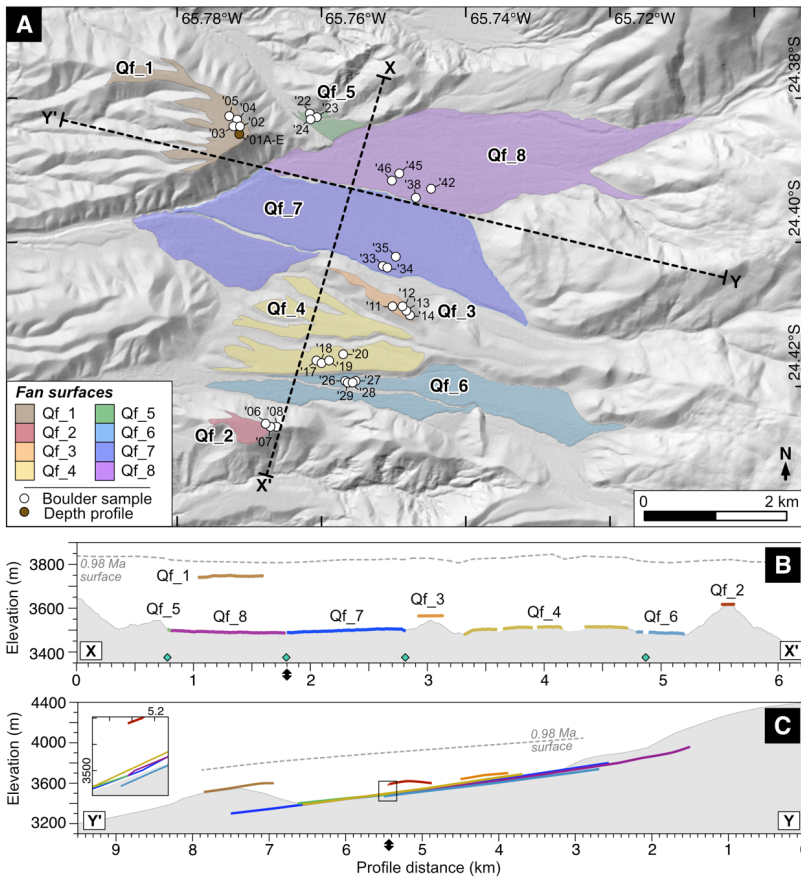
279 Supporting topographic, fan and channel data were extracted from the [digital elevation model \(DEM\)](#)
280 using TopoToolbox functions in MATLAB (Schwanghart and Scherler, 2014) and geospatial toolboxes
281 (GRASS, GDAL) in QGIS ([geographic information system software](#)). We also compiled a set of climate
282 (Berger and Loutre, 1991; Baker et al., 2001; Imbrie et al., 2006; Fritz et al., 2007; Wang et al., 2007;
283 Lisiecki and Raymo, 2009), paleoenvironmental (Hilley and Strecker, 2005; Tofelde et al., 2017; Pingel
284 et al., 2020), glacial (Martini et al., 2017; Zech et al., 2017; Luna et al., 2018; D’Arcy et al., 2019a;
285 Mey et al., 2020) and geomorphic (Terrizzano et al., 2017; Tofelde et al., 2017; Pingel et al., 2019b;
286 Tobal et al., 2021; Peri et al., 2022; Milanez Fernandes, 2023) records for the Andes to help
287 contextualise our results.

288

289 3.1 CRN dating

Deleted:
Formatted: Not Superscript/ Subscript

291 We collected a total of 30 quartzite boulder surface samples from eight fan surfaces (Fig. 3). Between
 292 three and four boulders were sampled per surface. Each surface was named 'Qf' for 'Quaternary fan',
 293 followed by a number which referred to its stratigraphic position. For example, Qf_1 sits ~200 m above
 294 the modern river channel, and as the highest elevation surface of the study area, it was anticipated to be
 295 the oldest fan.
 296



297
 298 **Figure 3.** Alluvial fan surfaces of the upper basin. A) Hillshade map of the dated fan surfaces with boulder and depth profile
 299 sampling locations shown. Sample names have been abbreviated (e.g.: TB19_05: '05). X-X' and Y-Y' linear projection lines
 300 of Fig. 3B and 3C are represented by dashed black lines. B) Fan sequence stratigraphy shown by fan surfaces projected onto
 301 X-X'. Qf_2 and Qf_3 surface widths are slightly exaggerated to improve visibility. Modern topography shaded in grey. The
 302 0.98Ma surface (grey dashed line) is modelled from sediment evacuation estimates of Hilley and Strecker (2005). Location of
 303 active fluvial channels indicated by green diamond symbol. C) Fan surfaces projected onto Y-Y'. Inset plot provides higher
 304 resolution view of projections (outlined by black rectangle). Projection line intersection is indicated by black double arrow.
 305

306 Each sampled boulder was embedded within the fan surface, located away from channels, and within
 307 the distal zone of the landform. This sampling strategy reduced the likelihood that the boulders were

Deleted:

309 sourced from adjacent hillslopes or were part of a depositional event following landform abandonment
310 (D'Arcy et al., 2019b; Orr et al., 2021). The sampled boulders were the largest, freshest boulders that
311 we were able to identify within the distal zone. However, we cannot definitively discount the possibility
312 that the boulders experienced some weathering, surface spallation or fracturing in the past.

313

314 We removed between 400 and 1000 g of sample from the upper three centimetres of each boulder
315 surface. The samples were crushed and then sieved to isolate the 250–500 µm grainsize fraction needed
316 for CRN dating. Sample cleaning, purification, [carrier addition](#), extraction and oxidation of Be, and
317 target preparation for AMS measurement was conducted in the Helmholtz Laboratory for the
318 Geochemistry of the Earth Surface (HELGES) at the German Research Centre for Geosciences (GFZ-
319 Potsdam) using the procedures outlined by von Blanckenburg [et al.](#), (2004) and Wittmann et al. (2016).
320 AMS measurements were completed at the Cologne AMS facility at the University of Cologne,
321 Germany.

322

323 Exposure ages derived from *in situ* produced ¹⁰Be concentrations were calculated using the CREp online
324 calculator (Martin et al., 2017) with the regional reference (SLHL [\[sea-level, high latitude\]](#)) production
325 rate of 3.74 (±0.09) at/ g yr for the high-elevation (> 3400 m asl) Central Andes (Blard et al., 2013;
326 Kelly et al., 2015; Martin et al., 2015), and the LSD ([Lifton-Sato-Dunai](#)) scaling scheme (Lifton et al.,
327 2014). Further information about the boulder samples, the CRN laboratory procedure, blank ratios, and
328 age calculation is provided in Supplement 1 and 2.

329

330 The probabilistic model for inferring the timing of fan surface abandonment from D'Arcy et al. (2019
331 b) was applied to fans with exposure ages of less than ca. 300 ka. The model uses the exposure ages of
332 boulders on the fan surface to generate a probability distribution of abandonment ages and a most
333 probable abandonment age. [The modelled abandonment age is based on the premise that an alluvial fan
334 surface remains active for a period of time that may generate a range of exposure ages exceeding the
335 uncertainty bounds on any individual age. The calculated abandonment age and its uncertainty is thus
336 dependent on the youngest measured exposure age, the duration of surface activity, and the number of
337 samples. For a detailed description of the approach, see D'Arcy et al., \(2019b\).](#) The model was not
338 applied to older fan surfaces, which have large age distributions (>100 kyr range) and likely have some
339 inheritance and/or surface erosion (Phillips et al., 1990; Tobal et al., 2021). Working with chronological
340 data at this coarse resolution over 10⁵-10⁶-year timescales means that even the most sophisticated
341 inheritance/erosion models are limited in their ability to estimate the timing of landform abandonment
342 (e.g., Prush and Oskin, 2020; Dortch et al., 2022). For the Toro fans where this applies, we use the age
343 distribution, stratigraphic order of the fans, and youngest exposure age as a guide for the timing of
344 abandonment.

Deleted: ¹⁰

Deleted: ,

Deleted: ⁻⁶

348

349 3.2 ¹⁰Be depth profile

350 To help substantiate our new ¹⁰Be boulder dataset we also resampled the Qf_1 ¹⁰Be depth profile,
351 referred to as P6b by Tofelde et al. (2017), and corresponding to their terrace level T6. The original
352 profile was limited to five samples, which were sampled over relatively broad depth intervals (0–10cm,
353 18–28 cm, 25–81 cm, 82–164 cm, 164–210 cm). To obtain more highly resolved ¹⁰Be data for this
354 surface, particularly in the upper 100 cm, five samples of > 65 pebbles each were extracted from the
355 following depth intervals (cm): 0–10, 20–30, 40–50, 60–70 and 115–125. The pebble samples were
356 crushed and sieved, and the 500–1000 µm fraction was reserved for CRN dating. Subsequent laboratory
357 procedures followed that of the boulder samples.

358

359 The Qf_1 ¹⁰Be depth profile, using combined ¹⁰Be data from this study and from Tofelde et al., (2017),
360 was used to determine an exposure age using the Hidy et al. (2010) Monte Carlo simulator. Further
361 details are provided in Supplement 1 and 2.

362

363 4. Results

364

365 We use the upper Toro Basin alluvial fan elevations, surface characteristics, and CRN ages to identify
366 two generations of fan surfaces. The studied fans are predominantly matrix-supported conglomerates
367 with sub-angular to rounded pebble and cobble clasts. Weathered desert pavements cap many of the fan
368 surfaces; a layer of finer sands and gravels are overlain by pebbles, cobbles, and boulders (e.g.,
369 McFadden et al., 1989; Tofelde et al., 2017).

370

371 The Generation 1 (G1) fan surfaces, comprising Qf_1 through 4, are stratigraphically the highest in the
372 record and are positioned ~200 to 50 m above the modern river channel(s) (Fig. 3). The fan surfaces are
373 moderately to highly weathered, with some evidence of surface boulder spallation (Fig. 4). With a few
374 rare exceptions, the G1 sampled boulders are smaller than those sampled from the lower Generation 2
375 (G2) surfaces. The G1 and G2 boulders have b-axis lengths which range from 30 to 80 cm and 30 to
376 140 cm, respectively (Supplement 2). The CRN exposure ages from the G1 surfaces range between ca.
377 970 and 340 ka (Table 1; Fig. 5, 6).

378

379 G2 is comprised of fans Qf_5 through 8, which have surfaces within 10 m elevation of the modern
380 channel(s) (Fig. 3). These moderately weathered surfaces retain debris flow deposits, evidence of past
381 channel avulsion and sparse human infrastructure (e.g., stone walls). The CRN exposure ages of this
382 younger fan generation range between ca. 100 and 20 ka, with estimated surface abandonment ages
383 after ca. 70 ka (Table 1; Fig. 7).

384

Deleted: ¶

Deleted: ¶

B93
B94

Table 1. Sample properties, measured *in situ* ¹⁰Be concentrations and calculated exposure ages of each sampled boulder from the Toro fans. Further sample and age calculation details are provided in the Supplement 2 and 3.

Sample	Location			Sample thickness (cm)	Shielding correction	Be-10 concentration		Be-10 exposure ages ¹	
	Latitude (°S)	Longitude (°W)	Elevation (m asl)			Concentration (10 ⁶ at/g SiO ₂)	Uncertainty (10 ⁶ at/g SiO ₂)	Age (ka)	Uncertainty (ka)
Qf_1									
TB19_02	-24.38492	-65.76890	3556	1	0.990	24.20	0.78	966.63	109.78
TB19_03	-24.38492	-65.76890	3556	1	0.990	16.02	0.52	593.11	59.10
TB19_04	-24.38492	-65.76890	3556	1	0.990	22.33	0.72	884.41	95.34
TB19_05	-24.38492	-65.76890	3556	1	0.990	16.97	0.55	639.17	63.94
Qf_2									
TB19_06	-24.42522	-65.76775	3560	1	0.999	11.36	0.37	391.94	37.91
TB19_07	-24.42566	-65.76682	3570	2	0.999	17.00	0.55	631.77	64.10
TB19_08	-24.42568	-65.76607	3581	2	0.999	10.18	0.33	336.94	33.17
Qf_3									
TB19_11	-24.40882	-65.75023	3644	1	0.998	15.45	0.50	533.56	52.88
TB19_12	-24.40918	-65.74864	3658	3	0.998	18.06	0.59	651.82	66.21
TB19_13	-24.40976	-65.74810	3660	3	0.998	17.77	0.58	634.67	64.63
TB19_14	-24.41011	-65.74773	3673	3	0.998	11.18	0.37	361.38	35.49
Qf_4									
TB19_17	-24.41665	-65.76059	3509	1	0.999	14.73	0.48	548.44	54.60
TB19_18	-24.41675	-65.76000	3512	2	0.999	17.26	0.56	679.67	68.23
TB19_19	-24.41654	-65.75923	3519	3	0.999	19.06	0.61	778.81	79.15
TB19_20	-24.41533	-65.75681	3541	1	0.999	21.41	0.69	847.34	90.30
Qf_5									
TB19_22	-24.38245	-65.76145	3404	2	0.990	2.02	0.07	70.63	6.28
TB19_23	-24.38263	-65.76109	3407	2	0.995	2.34	0.08	82.69	7.35
TB19_24	-24.38275	-65.76144	3405	3	0.995	2.77	0.09	98.81	8.82

Formatted: Font: Italic

Deleted: ¶

Qf_6

TB19_26	-24.41923	-65.75623	3531	2	0.998	2.16	0.07	69.97	6.27
TB19_27	-24.41921	-65.75578	3532	1	0.998	2.52	0.08	81.85	7.31
TB19_28	-24.41924	-65.75569	3541	2	0.998	2.22	0.08	71.11	6.46
TB19_29	-24.41941	-65.75652	3525	3	0.998	2.47	0.08	82.00	7.33

Qf_7

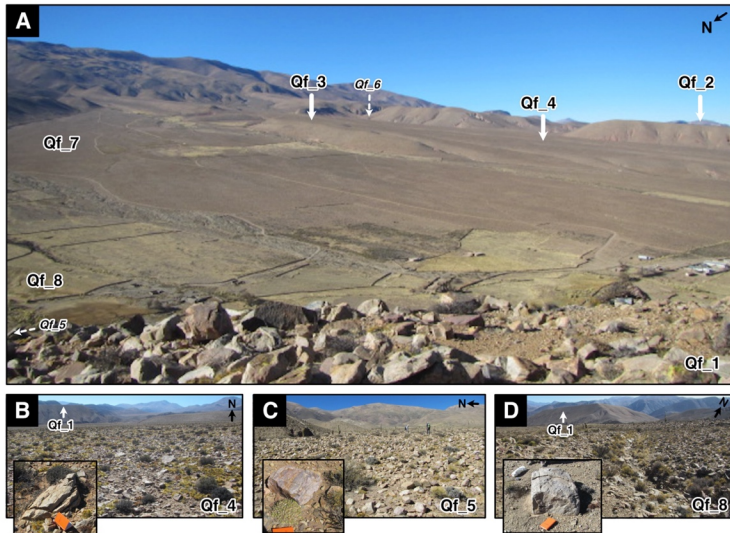
TB19_33	-24.40346	-65.75108	3557	1	0.998	1.22	0.04	38.78	3.46
TB19_34	-24.40371	-65.75107	3555	2	0.998	1.87	0.06	59.28	5.36
TB19_35	-24.40203	-65.74977	3563	3	0.998	2.11	0.07	66.94	6.13

Qf_8

TB19_38	-24.39402	-65.74711	3533	1	0.997	1.43	0.05	44.34	4.08
TB19_42	-24.39275	-65.74500	3553	1	0.997	1.43	0.05	43.65	4.04
TB19_45	-24.39043	-65.74940	3510	1	0.997	0.63	0.02	22.37	1.85
TB19_46	-24.39140	-65.75027	3502	1	0.997	1.44	0.05	45.32	4.212

1: LSD scaling scheme (Lifton et al., 2014), ERA40 Atmosphere Model (Uppala et al., 2005), LSD framework for geomagnetic correction (Lifton et al., 2014), Reference (SLHL) production rate: 3.74±0.09 at/g/yr. Sample density: 2.75 g cm⁻³. Erosion: 0 mm yr⁻¹

396
397
398
399
400
401
402
403
404
405
406



408

409 **Figure 4.** Images of the alluvial fan sequence of the upper Toro Basin. A) Image taken from Qf_1 surface (facing SE) with
 410 fan surfaces labelled. Italicized text with arrows indicates location of surfaces that are not clearly in shot. B) Qf_4 surface.
 411 Inset image of sampled boulder TB19_19. C) Qf_5 surface. Inset image of sampled boulder TB19_22. D) Qf_8 surface. Inset
 412 image of sampled boulder TB19_44. Images B–D encompass full age range of sampled surfaces. Further images of the fan
 413 surfaces and ^{10}Be samples are provided in Supplement 3.

414

415 4.1 Generation 1

416 Qf_1 is the highest fan surface of the record (~200 m above the modern channel), which extends from
 417 the Quebrada Rosal tributary catchment. The fan comprises part of the Quaternary conglomerates,
 418 which overlie the Barres Sandstone Formation (Fig. 2, 3). The depth profile is composed of four
 419 sedimentary units that coarsen with depth: silts and fine sands (0–20 cm), fine-coarse sand (20–60 cm),
 420 coarse sand and gravel (60–180 cm) and gravels (>180 cm). Consistent with the original profile, the
 421 new ^{10}Be sample concentrations decrease exponentially with depth (Fig. 5; Table 2). Qf_1 has a
 422 Bayesian most-probable exposure age of 715.8^{+35}_{-217} ka (2σ upper age: 750.8 ka, 2σ lower age: 498.8
 423 ka) and $0.26 \pm 0.42 \times 10^6$ atoms/g of inheritance. Within the simulator, we constrained fan surface erosion
 424 and inflation by setting the erosion rate to range between -0.02 and 0.2 cm/ka and using maximum and
 425 minimum erosion thresholds of -10 and 50 cm, respectively. While this modelled exposure age is
 426 consistent with the age estimated earlier by Tofelde et al. (2017) of 732^{+53}_{-56} ka assuming a stable
 427 surface, or 644^{+43}_{-49} ka accounting for surface inflation, Tofelde et al. (2017) preferred the exposure
 428 age they derived from surface pebbles of 453 ± 33 ka.

429

430 The exposure ages of boulder samples TB19_03 and TB19_05 are in agreement with the depth profile
 431 results, yielding exposure ages of 639.17 ± 63.94 and 593.11 ± 59.10 ka (2σ uncertainty). The two

432 remaining boulders (TB19_02, TB19_04) yielded older exposure ages of 966.63 ± 109.78 and 884.41
 433 ± 95.34 ka.

434

435 **Table 2.** Sample depths and measured ^{10}Be concentrations of Qf_1 depth profile. Fan age calculated with the Hidy
 436 et al. (2010) Monte Carlo depth profile simulator was 715.8^{+357}_{-217} ka. Inheritance measured: $0.26 \pm 0.42 \times 10^6$
 437 at/g SiO_2 .

Formatted: Justified

Deleted: ¶

Formatted: Subscript

Sample ¹	Sample depth		Be-10 concentration	
	Depth (cm)	Uncertainty (cm)	Concentration (10^6 at/g SiO_2)	Uncertainty (10^6 at/g SiO_2)
BBC-0	5	5	14.70	0.18
TB19_01A	5	5	14.97	0.48
BBC-1	23	5	11.80	0.11
TB19_01B	25	5	12.14	0.39
TB19_01C	45	5	10.88	0.35
BBC-2	53	28	7.76	0.07
TB19_01D	65	5	8.76	0.28
TB19_01E	120	5	4.94	0.16
BBC-3	123	41	5.21	0.06
BBC-4	187	23	2.30	0.03

438 ¹: TB19_01A-E from this study. 'BBC-1-4' from Tofelde et al. (2017).

439

440 Surface Qf_2, the second highest surface (ca. 130 m above the closest modern channel), also overlies
 441 the Barres Sandstone and likely extends from the Quebrada Huasa Ciénaga and Quebrada del Chorro
 442 catchments. CRN exposure ages from three boulders range from 631.88 ± 64.10 to 336.94 ± 33.17 ka.

443

444 The Qf_3 surface is positioned ca. 60 m above the closest modern channel and extends from the
 445 Quebrada Rosal tributary catchment. The surface yields three CRN boulder exposure ages that cluster
 446 between 651.82 ± 66.21 and 533.56 ± 52.88 ka, and one younger age of 361.38 ± 35.49 ka.

447

448 Qf_4 has a highly dissected fan surface which is the lowest stratigraphically of the G1 fans; the fan is
 449 positioned ca. 40 m below the Qf_3 surface and ca. 30 m elevation above the modern channel. Four
 450 boulder exposure ages range from 911.61 ± 100.27 to 548.44 ± 54.60 ka.

451

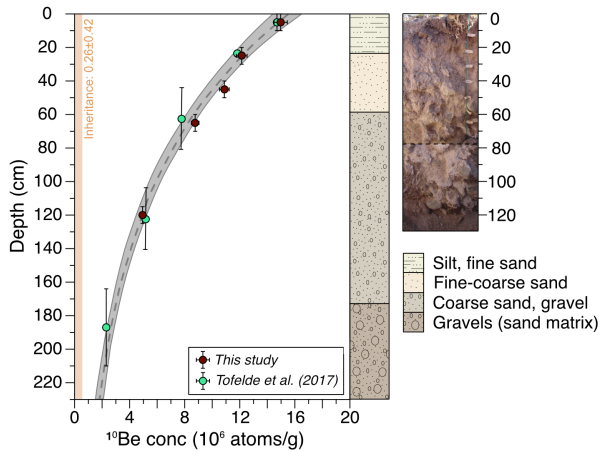
452 4.2 Generation 2

453 Qf_5 is a small G2 surface that sits ca. 10 m above the neighboring Qf_8 fan. Qf_5 has three exposure
 454 ages that range from 98.81 ± 8.82 to 70.63 ± 6.28 ka, with a most probable abandonment age of 61.8
 455 $^{+13.5}_{-33.6}$ ka (no ages excluded as outliers).

456

457 Qf_6's surface is characterized by moderately weathered debris flow deposits with clusters and
 458 elongated ridges of boulders. Exposure ages range between 82.00 ± 7.33 and 69.97 ± 6.27 ka from the

460 four boulders, with an estimated surface abandonment age of $66.2^{+11.0}/_{-17.5}$ ka (no ages excluded as
 461 outliers).



462
 463 **Figure 5.** ^{10}Be concentration with depth for Qf_1 profile alongside sedimentary log and stitched field image of the profile pit.
 464 Each sample was collected over a depth range represented by a vertical error bar. Horizontal error bar represents the 1σ
 465 analytical uncertainty for the nuclide concentration. The Hidy et al. (2010) Monte Carlo simulator fit 100,000 curves (grey
 466 shading) to profile and generated most probable fit (grey dashed line). Modelled inheritance is shown by orange line. *Profile
 467 6b data, rather than 6a, from the supplementary materials is used in simulation, due to the mislabelling of the profile in Fig. 4
 468 of Tofelde et al. (2017).
 469

470 Despite Qf_7 being located within 5 m elevation of the youngest G2 fan Qf_8, this large fan appears
 471 more weathered than Qf_8. Qf_7 has CRN exposure ages of 66.94 ± 6.13 , 59.28 ± 5.35 and $38.78 \pm$
 472 3.47 ka. The surface abandonment ages including and excluding the youngest age are $33.9^{+7.4}/_{-25.1}$ and
 473 $52.9^{+11.0}/_{-16.3}$ ka, respectively.

474
 475 Surface Qf_8 yielded a cluster of older ages that range between 45.32 ± 4.2 and 43.65 ± 4.04 ka and a
 476 single younger age of 22.37 ± 1.83 ka. Abandonment ages including and excluding the youngest age
 477 are $19.4^{+4.1}/_{-19.4}$ and $42.4^{+6.5}/_{-7.5}$ ka, respectively. The surface is covered with relatively unweathered
 478 debris flow deposits and large varnish-free boulders.

479
 480 **5. Discussion**

481
 482 While there are some nuances to the Toro Basin fan record, our new CRN dataset enables us to identify
 483 significant phases of net incision since ca. 0.98 Ma, capture the channel response to external forcing
 484 over a range of timescales and cyclicities, and gain further insight into the late Quaternary evolution of
 485 the Toro Basin.

486

487 **5.1 Timing of alluvial fan development and abandonment**

488 CRN age uncertainties on the order of 10^4 – 10^5 years and a wide range of fan exposure age distributions
489 on individual surfaces present some challenges when interpreting the Toro fan chronostratigraphy,
490 which is crucial for comparison with potential external forcing conditions. Constraining the geological
491 uncertainties of the CRN ages, particularly for old fan surfaces, is often challenging (Owen et al., 2014).
492 For this reason, we use geological, topographic and paleoenvironmental data alongside the ^{10}Be data to
493 interpret the alluvial fan record. The coarse resolution of the G1 ^{10}Be record means that while we can
494 reflect upon long term shifts in channel behaviour for the upper Toro Basin, we must exercise caution
495 when linking this record to specific forcing or events (Gray et al., 2014; Dühnforth et al., 2017; Orr et
496 al., 2021). Pairing the ^{10}Be record with cosmogenic ^{21}Ne in the future may help to decipher some of the
497 complexities in the exposure histories of the boulders; ^{21}Ne is well suited for quantifying long term
498 landscape change in arid, low erosion environments (Dunai et al., 2005; Ma and Stuart, 2018).

499

500 *5.1.1 Fan Generation 1*

501 The ~200-m elevation difference between the highest and lowest fan surface among Generation 1 means
502 that the G1 surfaces could not have been active simultaneously (Fig. 6). Substantial inheritance and/or
503 erosion has therefore likely affected individual boulders from these surfaces and offers one explanation
504 for the broad spread in ages (>400 kyr) for each.

505

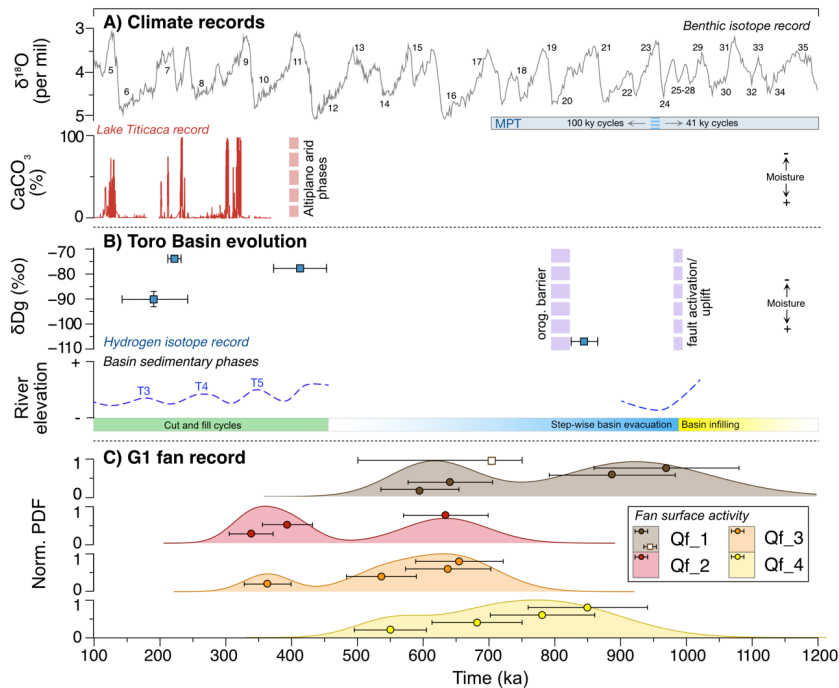
506 Pairing the Qf_1 ^{10}Be depth profile with the surface boulder exposure ages means that we can more
507 robustly constrain the oldest phase of fan development within the study area and use it as a benchmark
508 when evaluating the remainder of the G1 fan record. The most recent phase of Qf_1 surface activity
509 and/or stability is constrained by the depth profile data and two boulders to between ca. 750 and 600
510 ka. In this case, we believe that CRN inheritance may explain why the remaining two boulders
511 (TB19_02, TB19_04) from this surface yield exposure ages that exceed ca. 800 ka. Considering the
512 whole suite of boulder ages for the G1 fans, which mostly exceed 500 ka, we find it unlikely that the
513 age of 453 ± 33 ka (based on surface pebbles) originally reported by Tofelde et al. (2017) for Qf_1 is
514 correct.

515

Deleted: -5

Formatted: Not Superscript/ Subscript

Formatted: Not Superscript/ Subscript

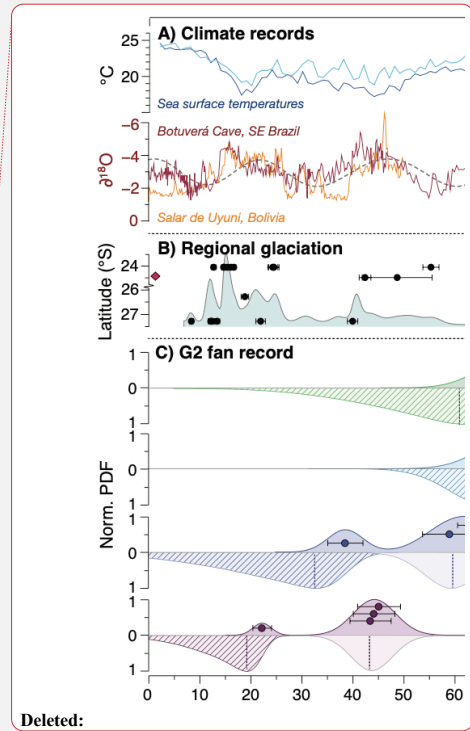
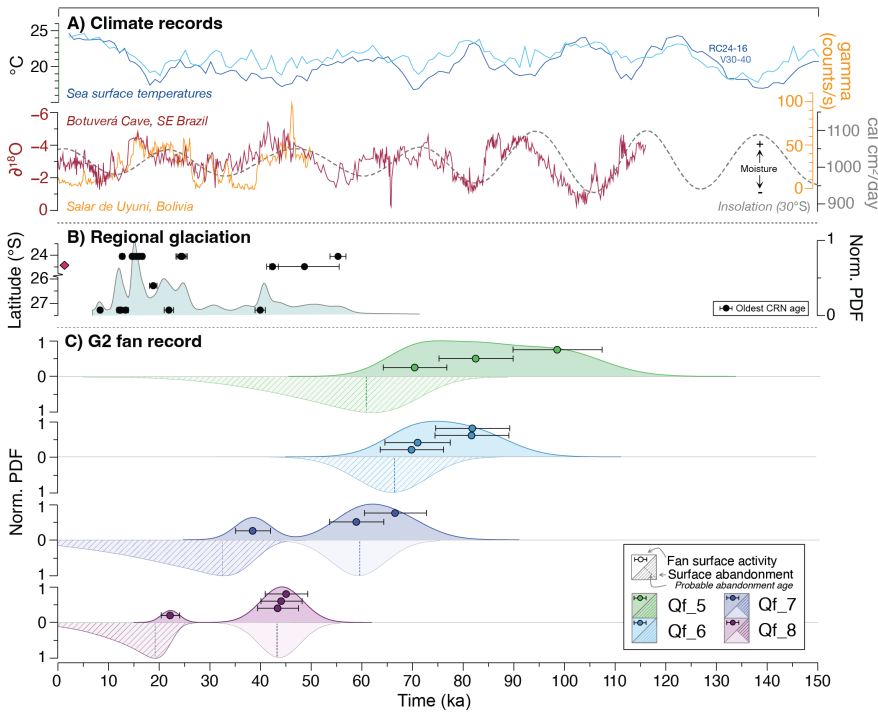


517 **Figure 6.** Comparison between the G1 fan ^{10}Be dataset and records of Toro Basin evolution and climate. A) Benthic isotope record (Lisiecki and Raymo 2009) displayed alongside Marine Isotope Stages (MIS) and Mid-Pleistocene Transition labelling and the Lake Titicaca sediment core record (CaCO_3 concentration) from Fritz et al. (2007). B) Toro basin evolution. Climatic variability represented by hydrogen isotope record of Pingel et al. (2020). Basin sedimentary and tectonic phases plotted with respect to inferred river elevation over time, as observed by this study and described by Hilley and Strecker (2005), Tofelde et al. (2017) and Pingel et al. (2020). Fluvial terrace record (T3-6) from Tofelde et al. (2017). C) ^{10}Be surface boulder ages and normalised probability density functions (PDFs) of the G1 surfaces. Horizontal error bars represent the 1σ uncertainty for the exposure ages. Bayesian modelled surface age of Qf_1 (715.8^{+35}_{-217} ka) derived from depth profile (Fig. 5) is denoted by square point.

527 Given the stratigraphic positions of Qf_2 and Qf_3, it is unlikely that active streams were present on these surfaces after ca. 400 ka. For this reason, we suggest that the younger ages for these surfaces are the result of erosion. These surfaces also must be older than surface Qf_4, which yielded a youngest age of ca. 550 ka.

531 Inheritance also likely explains the old (>750 ka) boulders on Qf_4, which is stratigraphically younger than Qf_1 and cannot have been active at the same time.

Deleted: we think that



535

536 **Figure 7.** Comparison between the G2 fan ¹⁰Be dataset and regional climate and glacial records. A) Climate records. Sea
 537 surface temperatures from Imbrie et al. (2006), insolation from Berger and Loutre (1991), Botuverá Cave, SE Brazil
 538 speleothem record from Wang et al. (2007) and Salar de Uyuni, Bolivia lake record from Baker et al. (2001). B) CRN glacial
 539 chronologies from the Central Andes (see Fig. 1A for location): Nevado de Chañi (24°S, 65.7°W, Martini et al., 2017, Mey
 540 et al., 2020), Quevar Volcano (24.4°S, 66.8°W, Luna et al., 2018), Sierra de Quilmes (26.2°S, 66.2°W, Zech et al., 2017) and
 541 the Sierra Aconquija (27.2°S, 66.1°W, D'Arcy et al., 2019a). Location of Toro Basin (24.4°S, 66.7°W) is indicated by red
 542 diamond symbol. C) ¹⁰Be surface boulder ages and normalised probability density functions of the G2 surfaces. Horizontal
 543 error bars represent the 1σ uncertainty for the exposure ages. Normalised PDF of fan surface abandonment (hashed shading)
 544 calculated using the D'Arcy et al. (2019b) probabilistic model for fan surface abandonment. Surface abandonment for Qf_7
 545 and Qf_8 without youngest boulder ages (TB19_33 and TB19_45, respectively) shown by PDFs with opaque solid shading.
 546 Most probable abandonment ages denoted with dashed vertical lines- Qf_5: 61.8^{+13.5}/_{-33.6} ka, Qf_6: 66.2^{+11.0}/_{-17.5} ka, Qf_7: ca.
 547 33.9^{+7.4}/_{-25.1} ka (52.9^{+11.0}/_{-16.3} ka), Qf_8: 19.4^{+4.1}/_{-19.4} ka (42.4^{+6.5}/_{-7.5} ka).
 548

549 Given these complexities in the fan chronostratigraphy, rather than identifying discrete phases of
 550 aggradation and incision for each fan surface, we suggest that the G1 fan record can instead be used to
 551 capture an extended phase of net incision within the Sierra de Pascha tributaries. Crucially, this is
 552 unlikely continuous incision, but rather a phase of net incision, which was punctuated by the formation
 553 of individual surfaces, possibly controlled by higher frequency climate cyclicity (e.g. 100-kyr). If so,
 554 this would imply periods of faster incision through the fill. By comparing the G1 fan record with the
 555 modelled palaeotopography of Hilley and Strecker (2005), we estimate that ~100 m of net incision
 556 (~0.01 mm/yr) occurred within the upper basin between ca. 0.98 Ma and 800 ka, at which point the
 557 Qf_1 surface became active (Fig. 3B, C, Fig. 8). Approximately 200 m of net incision (~0.07 mm/yr)

Deleted:

563 then followed between ca. 800 ka and the complete abandonment of the G1 fans by ca. 500 ka (when
564 adjusting for age outliers) (Fig. 6), which signals the significant stepwise evacuation of sediment from
565 the upper Toro Basin at this time.

566

567 *5.1.2 Fan Generation 2*

568 The G2 record reveals that after a hiatus in the geomorphic record ca. 500 and 100 ka, fan aggradation
569 and incision is recorded throughout several of the Sierra de Pascha tributaries (Fig. 8). Rather than
570 recording continuous fan activity since ca. 110ka, the distribution of ages for G2 instead likely captures
571 multiple distinct phases of deposition. The G2 fan surfaces have much tighter constrained age
572 distributions (ca. 21 to 40 kyr) compared to the G1 fans, with two G2 fans showing what may be young
573 outliers; the boulders are therefore less likely to be affected by inheritance, but the young outliers may
574 be affected by erosion or tilting by human or animal activity.

575

576 **5.2 Drivers of alluvial channel system change and fan/terrace formation**

577 Before we can explore some of the possible explanations for the alluvial system change recorded in the
578 Toro Basin, we must first consider the specific local conditions needed to help explain the G1 (ca. 800
579 to 500 ka) and G2 (ca. 100 to 20 ka) fan generations in the upper basin, as well as the fluvial terrace
580 sequence (ca. 370 ka to <75 ka) in the lower basin. Changes in water or sediment discharge, governed
581 by climate, can affect channel slopes and prompt adjustments to the channel bed elevations through
582 incision or aggradation (Howard, 1982; Wickert and Schildgen, 2019; Tofelde et al., 2019).
583 Nevertheless, net incision is essential to preserving the geomorphic record of aggradation-incision
584 cycles. Otherwise, subsequent aggradational phases are likely to bury earlier landforms. Net incision
585 can occur through the channel response to ongoing rock uplift or base level fall (Simpson and
586 Castelltort, 2012), the latter of which may include renewed incision through an aggraded sequence of
587 sediment downstream. While autogenic processes, such as channel avulsion and meander cut-offs may
588 also play a role in channel incision and the formation of discrete fan lobes or terraces (Nicholas and
589 Quine, 2007; Ventra and Nichols, 2014), we consider the scale of channel incision associated with the
590 features of interest (ranging from ca. 10 to hundreds of meters) is beyond the scope of purely autogenic
591 behavior. Below, we consider how climate-modulated changes to water and sediment discharge,
592 together with events that can drive net incision, may have helped to generate, and preserve multiple
593 generations of fans and terraces within the Toro Basin.

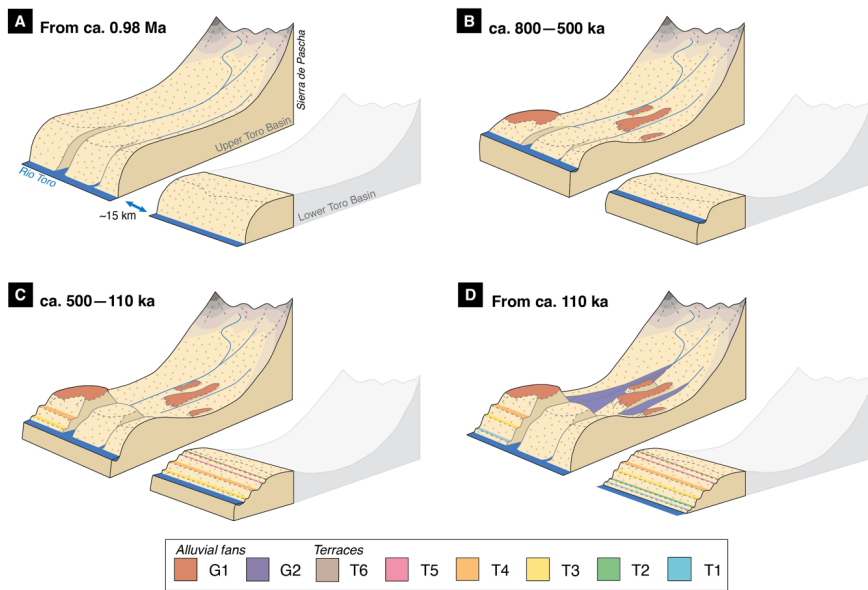
594

595 *5.2.1 Fan formation from ca. 800 to 500 ka*

596 The development, entrenchment, and eventual abandonment of the G1 fans could be part of the
597 landscape response to enhanced rock-uplift of the Sierra de Pascha Sur, starting no later than ca. 800 ka
598 (Fig. 8) (Clarke et al., 2010; Mather et al., 2017; Mouchené et al., 2017). However, another mechanism
599 is likely at play because the averages rates of incision between ca. 800 and 500 ka (0.8 mm/yr) as

600 recorded by the G1 fans, exceed the estimated rock uplift rates of 0.4 – 0.6 mm/yr (Hilley and Strecker,
 601 2005), and tectonic uplift alone is unlikely to be pulsed in a manner that would generate multiple fans.
 602 More likely, both climate forcing and tectonic forcing combine to produce and preserve the G1 fan
 603 sequence. Over the same period, curiously, no terraces are detected in the lower Toro Basin. Three
 604 possible explanations for this absence (which are not mutually exclusive) include: (1) due to their more
 605 central position within the basin, the lower reaches of the Río Toro were not strongly affected by rock
 606 uplift, meaning that any changes in river-channel elevation are not persevered in the geomorphic record
 607 due to low or a lack of net incision; (2) channels in the lower Toro Basin continued to experience
 608 aggradation or remained stable at this time, due to feedbacks in the system whereby incision upstream
 609 caused a pulse of sediment for downstream reaches; or (3) the response time of the Río Toro within the
 610 lower basin was substantially longer than the forcing period of the aggradation-incision cycles, meaning
 611 perturbations to the channel-bed elevation due to climate forcing would not have reached so far
 612 downstream.

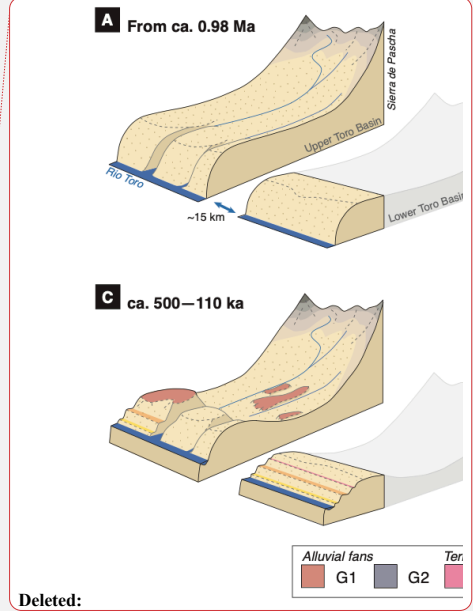
613



614

615 **Fig. 8.** Cartoon illustrating periods of aggradation and incision in the upper and lower Toro Basin from ca. 0.98 Ma (also see
 616 Table 3). Area of Lower Toro Basin block shaded in grey was not part of this study. A) From 0.98Ma: Base level lowered to
 617 present day levels, following the deposition of Alfarcito Conglomerates. Renewed hydrological connectivity likely led to
 618 extensive sediment evacuation and incision of (paleo)topography. Deposition of Quaternary Terrace Conglomerates started
 619 from 0.94 Ma (Hilley and Strecker, 2005). B) ca. 800-500 ka: G1 fan formation and abandonment during a phase of net incision
 620 in the upper basin, linked to the MPT. **Aggradation was recorded in the lower basin (Tofelde et al., 2017).** C) ca. 500-110 ka:
 621 100-kyr cycles of aggradation and incision recorded by lower basin cut-and-fill terraces (T6 [ca. 490–450 ka], T5 [ca. 370 ka],
 622 T4 [ca. 285–260 ka], T3 [ca. 170 ka]). No significant geomorphic change recognised in the tributaries of the upper basin. D)
 623 From ca. 110 ka: G2 fan formation and abandonment in the upper basin, linked to ca. 21/40 kyr climate cycles. Continuation
 624 of 100-kyr cycles recorded by lower basin terraces (T2 [ca. 110–75 ka], T1 [< 75 ka]).

Deleted:



Deleted:

Deleted: No significant geomorphic change recognised in the lower basin.

Deleted:

630
631

Table 3. Summary of upper and lower Toro Basin evolution

	<u>UPPER BASIN</u>		<u>LOWER BASIN</u>	
	<u>Process/event</u>	<u>Hypotheses (not mutually exclusive)</u>	<u>Process/event</u>	<u>Hypotheses (not mutually exclusive)</u>
<u>From ca. 0.98 Ma</u> <u>(Fig. 8A)</u>	<u>Base level lower than modern</u>	<u>(i) Renewed hydrological connectivity triggers incision</u>	<u>Base level lower than modern</u> <u>Deposition of 'Terrace Conglomerates'</u>	<u>(i) Renewed hydrological connectivity triggers incision</u> <u>(i) Uplift-induced basin infilling</u>
<u>ca. 800–500 ka</u> <u>(Fig. 8B)</u>	<u>Net incision recorded by G1 fan sequence</u>	<u>(i) Enhanced glacial cycles trigger incision</u> <u>(ii) Uplift of Sierra de Pascha Sur</u>	<u>Stability / continued deposition</u>	<u>(i) Lower reaches minimal affected by uplift</u> <u>(ii) System feedbacks promote stability/aggradation</u> <u>(iii) Response time exceeds forcing period</u>
<u>ca. 500–110 ka</u> <u>(Fig. 8C)</u>	<u>No activity recorded</u>	<u>(i) Restricted hydrological connectivity</u> <u>(ii) Downstream incision not yet propagated to upper basin</u>	<u>100-kyr cut-and-fill sedimentary cycles and net incision recorded by fluvial terraces</u>	<u>(i) Eccentricity-driven climate forcing, with continued uplift</u> <u>base-level drop causing net incision</u>
<u>From ca. 110 ka</u> <u>(Fig. 8D)</u>	<u>G2 fan aggradation-incision cycles and net incision</u>	<u>(i) Surface abandonment during intensified SASM/glacial periods</u>		

659
660
661
662
663
664
665
666
667
668
669
670
671
672

Formatted: Width: 29.7 cm, Height: 21 cm

Formatted Table

673 To elaborate on the first possibility, the Sierra de Pascha catchments are positioned behind and
674 perpendicular to west-tilted and deformed basin strata (Barres Sandstone, Agujas and Alfracito
675 Conglomerates, lava flows) (Fig. 2A). In concert with the work by Hilley and Strecker (2005), we
676 suggest that channel incision through the resistant sedimentary units accelerated sometime between
677 0.98 and 0.8 Ma. Once this incision propagated upstream, the removal of weakly consolidated
678 sedimentary units in the upper basin was likely efficient (Hilley and Strecker, 2005). This evolving
679 topography could therefore help to explain the net incision needed in the upper Toro Basin to preserve
680 the alluvial fan surfaces between ca. 800 to 500 ka, and why terrace levels in the lower basin are not
681 recognised during this time interval.

682

683 To elaborate on the second and third possibilities, as late Quaternary glaciations were limited to the
684 Pascha tributary headwaters (< 5 km from headwall), the hillslope geomorphic response to prolonged
685 and intensified glaciation may have been very localized (Tofelde et al., 2018). This is apparently true
686 for the Iglesia and Calingasta Basins in the Western Precordillera where the tributaries, rather than the
687 main basin record incision following the Mid-Pleistocene Transition (Terrizzano et al., 2017; Peri et al.,
688 2022). Following this argument, the response time of the Río Toro's long profile to the 100-kyr climate
689 cycles after the Mid-Pleistocene Transition (ca. 1.2 to 0.8 Ma) may have been substantially longer than
690 the period of external forcing. If true, this implies that while upstream reaches of the channel may have
691 experienced no (or a very low amplitude) aggradation/incision cycles (Allen, 2008; McNab et al., 2023).
692 Alternatively, feedbacks within the system could lead to differences not only in the magnitude of
693 aggradation/incision, but also the timing. For example, in southwest Peru, Steffan et al. (2009, 2010),
694 interpreted aggradation in downstream reaches of river channels during past wet climate periods to
695 result from pulses of sediment mobilized from hillslopes and upstream channel incision.

696

697 5.2.2 Terrace formation from ca. 500 to 110 ka

698 From ca. 500 to 110 ka in the upper Toro Basin, we find no record of fan formation (Fig. 8). Curiously
699 again, though, the lower Toro Basin exhibits a spectacular sequence of terraces showing 100-kyr
700 cyclicity starting from ca. 500 ka (Tofelde et al., 2017). If long channel response times explain the lack
701 of terraces from ca. 800 – 500 ka in the lower Toro Basin, to explain the terraces identified in the lower
702 basin ca. 500 ka (Tofelde et al., 2017), the channel response time must have changed. This could have
703 occurred as a result of incision in the upper Toro Basin, which would have narrowed the upstream river
704 valleys, consequently decreasing river response times and enabling aggradation-incision cycles to affect
705 channel reaches farther downstream (e.g., McNab et al., 2023).

706

707 While a shortened channel response time can explain the formation of terraces in the lower Toro Basin,
708 it does not explain the absence of terraces/fans in the upper basin over the same period. Consequently,

Deleted: ¶

Formatted: Section start: New page

Deleted: to the axis of an elevated northward-plunging anticline ...

Deleted: anticline

Deleted: and to the east of the anticline

Deleted: e

Deleted: of the anticline

716 we next consider other factors that might lead to differences in fan/terrace preservation between the
717 upper and lower Toro basins.

718

719 Perturbations at the Río Toro outlet, such as a shift in base level, will propagate upstream over time,
720 thus driving the net incision needed to preserve variations in channel bed elevation in the terrace and
721 fan sequences. Alternatively, activity along the Gólgota Fault at this time may have adjusted the base
722 level for the trunk stream. Regardless of the exact trigger for base-level fall (e.g., renewed fluvial
723 connectivity, possibly enhanced by a drop in Lerma Valley lake level) (Malamud et al., 1996; González
724 Bonorino and Abascal, 2012), a net incisional wave would have propagated upstream from the lower
725 basin or outlet. That incision would have facilitated terrace preservation in the lower Toro Basin before
726 the incisional wave propagated upstream to the upper Toro Basin. Steepened reaches of both the trunk
727 stream and tributaries up to an elevation of ca. 3400 m (Fig. 2C) are consistent with an upstream
728 propagating wave of incision, which probably only recently reached the ca. 3300-m elevation of the G2
729 fan toes.

730

731 Consistent with this interpretation, both the upper and lower Toro basins preserve geomorphic evidence
732 of channel-bed elevation lowering after ca. 100 ka (terraces T2 and T1 in the lower Toro Basin; G2 fan
733 generation in the upper Toro Basin). Whereas T2 and T1 lie 40 m and 20 m respectively above the
734 modern Río Toro, the G2 fans are at most 10 m above their closest channel. This finding further supports
735 the idea that net incision is ongoing in the lower Toro Basin, probably keeping pace with the ongoing
736 uplift of the Sierra de Pascha Sur (Tofelde et al., 2017), but net incision has possibly only resumed
737 within the last ca. 110 to 50 kyr in the upper Toro Basin.

738

739 Other factors may have also played a role in the misaligned timing of fan/terrace formation in the upper
740 and lower Toro basins. Restricted hydrological connectivity or disconnectivity can lead to internal
741 variability in the nature and timing of a basin's geomorphic or sedimentary response to external
742 perturbations (Fryirs et al., 2007; Buter et al., 2022). For example, basin connectivity and geometry
743 appear to have disrupted the timing of climate-driven sediment transfer within the Humahuaca Basin of
744 NW Argentina during the last glacial cycles, leading to anti-phased timing of aggradation-incision
745 cycles along tributaries on either side of the valley (Schildgen et al., 2016). No fault lines, which can
746 influence connectivity (Guarnieri and Pirrotta, 2008; Brocard et al., 2012), intersect the channel network
747 between the alluvial fans and terrace levels of the Toro Basin (Fig 2) (Pingel et al., 2020). Nevertheless,
748 minor adjustments to the long profile of an alluvial channel network can be sufficient to affect the
749 internal connectivity of a basin (Savi et al., 2020). One such adjustment may include the tributary
750 junction fan at the Quebrada de Chorro outlet, which has created a diffuse knickzone in the Río Toro
751 long profile (Fig. 2B). As the fan has aggraded, it has pushed the main channel to the opposite valley
752 side, evidenced by a marked channel bend. The fan may therefore inhibit the coupling between the

753 upstream and downstream reaches of the trunk stream by disrupting the flow of sediment and (possibly)
754 water from the Sierra de Pascha tributaries and along the Río Toro (e.g., Harvey 2012). However, the
755 capacity of the fan to disrupt environmental signals moving through the basin may depend on the
756 direction of signal travel. For example, channel incision due to a climate-induced increase in water
757 discharge may continue to propagate downstream, regardless of a new sedimentary input from a major
758 tributary, unless the tributary fully dams the upstream section. However, if a wave of incision is instead
759 migrating upstream, a tributary junction fan may slow or disrupt its propagation (Savi et al., 2020).
760 Nevertheless, while sedimentary inputs from individual tributaries can affect the modern channel
761 profile, and may slow upstream-propagating incisional cycles, it is not clear whether such localized
762 features will play an important role in channel network evolution over longer (e.g., > 100 kyr)
763 timescales.

764

765 *5.2.3 Fan formation since ca. 110 ka*

766 All G2 surfaces were either stable or actively receiving sediment for some time during both cool, wet
767 glacial periods and warm, dry interglacials. Similar to the terraces in the lower basin (Tofelde et al.,
768 2017), the timing of G2 surface abandonment is restricted to glacial phases; enhanced moisture
769 availability due to an intensified SASM is likely to have amplified sediment transport and channel
770 incision (Baker and Fritz, 2015). Around the latitude of the Toro Basin, glacial moraine records in the
771 Central Andes show strong evidence for glacial advances at ca. 16 and 22–24 ka, with some evidence
772 also for advances at ca. 42 and e.g. 20/55 ka (D’Arcy et al., 2019a; Fig 7B). The stratigraphically highest
773 surfaces in G2, Qf_5 and Qf_6, show abandonment ages that are consistent with the timing of the oldest
774 glacial advances recorded in the moraine record (ca. 55 ka).

775

776 For surfaces Qf_7 and Qf_8, the timing of abandonment is harder to interpret, due to the difficulty in
777 knowing whether the youngest boulders on each surface are outliers due to erosion/rotation, or if they
778 represent a time of active deposition on the surface. Given the similarities in surface weathering between
779 Qf_6 and Qf_7, it is possible that Qf_7 was active at the same time as Qf_6 and Qf_5, and hence was
780 abandoned at a similar time (implying that the youngest boulder of Qf_7 is an outlier). If the young
781 boulder instead represents a real depositional age, then the abandonment of Qf_7 could be linked to the
782 ca. 22–24 ka glacial advance, coinciding with the northern hemisphere Last Glacial Maximum. The
783 abandonment of Qf_8 is similarly challenging to interpret, with abandonment potentially linked to either
784 the ca. 24 ka glacial advance (associated with the ‘Minchin’ wet climate phase of the Central Andes) if
785 the youngest boulder is excluded, or the ca. 16 ka glacial advance associated with Heinrich Stadial 1 if
786 not excluded.

787

788 While we reason that the two youngest ages from Qf_7 and Qf_8 are not outliers and instead reflect
789 later deposition events (see 5.1.2), we have also estimated the timing of surface abandonment without
790 them (Fig. 7). In this alternative record, the abandonment of three of the four fans fall between ca. 65
791 and 60 ka. This points to a modest phase of net incision in several Sierra de Pascha catchments during
792 a dry interglacial period (Fritz et al., 2007).

Deleted: wet glacial

793
794 Overall, the exposure age distributions and estimated abandonment ages appear to capture cycles of fan
795 aggradation-incision with relatively high periodicity. Considering the above tentative links between
796 abandonment times and glacial advances, and that no known tectonic forcing in the Toro Basin can
797 explain this cyclicity, the alluvial channel network is likely responding to precession (21-kyr) or
798 obliquity-driven (40-kyr) climate cycles. Precessional forcing has been recorded within the sedimentary
799 archives elsewhere in the Central Andes, including fluvial terraces in the Humahuaca Basin (23°S)
800 (Schildgen et al., 2016) and alluvial fans in the Santa María Basin (26.5°S) (D'Arcy et al., 2018) in NW
801 Argentina.

Deleted: a periodicity of ca. 20 to 40 kyr

802

803 5.3 Impacts of the Mid-Pleistocene Transition on the Toro Basin

804 The G1 fan surfaces have CRN exposure ages that span several glacial-interglacial cycles (Fig. 6).
805 Although our interpreted ages are too imprecise to associate with specific glacial phases, 100-kyr glacial
806 moderation of aggradation-incision cycles is thought to have controlled fluvial terrace formation in the
807 lower Toro Basin (e.g., Tofelde et al., 2017). In semi-arid landscapes and transport-limited systems, this
808 finding is not unexpected, as geomorphic activity is invariably amplified during wetter, glacial periods
809 (Harvey et al., 1999; Spelz et al., 2008; Cesta and Ward, 2016). Given the number of G1 fans (n=4)
810 capturing the prolonged net incisional phase (>300 kyr), it is possible that eccentricity-driven cycles of
811 aggradation and incision are also recorded in the upper Toro Basin.

812

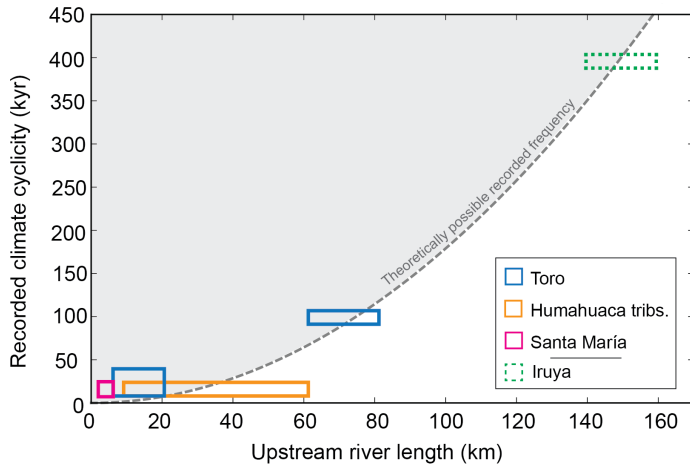
813 Our net incisional phase between ca. 800 and 500 ka coincides with the onset of prolonged and enhanced
814 global glacial cycles following the Mid-Pleistocene Transition (MPT, 1.2–0.8 Ma) which marked a shift
815 in climate periodicity from 41 to 100 kyr cycles (Berger et al., 1999). The southward migration of the
816 ITCZ at this time led to heightened moisture availability throughout the Central Andes (Haselton et al.,
817 2002; Broccoli et al., 2006; Vizzy and Cook, 2007). Alluvial channels in semi-arid regions of the Central
818 Andes are found to respond quickly to marked shifts in precipitation such as this (e.g., Schildgen et al.,
819 2016; Tofelde et al., 2017), which also appear to drive phases of enhanced sediment evacuation to the
820 foreland (Fisher et al., 2023).

821

822 Enhanced incision likely linked to the MPT has also been recognised at other locations in the Central
823 Andes (Fig. 1A), including the Casa Grande Basin (23°S) in the Eastern Cordillera, the Salinas Grandes

826 Basin (23.5°S) of the Puna Plateau (Pingel et al., 2019b), and the Iglesia (30.5°S) and Calingasta (32°S)
 827 basins in the Western Precordillera (Terrizzano et al., 2017; Peri et al., 2022). These observations point
 828 to a regional phase of net incision and therefore landscape response to global climate change. For several
 829 of these locations, including the Toro Basin, local tectonic activity may have provided a secondary
 830 driver for incision, or created conditions conducive to fan/terrace preservation. Towards the Andean
 831 interior, the geomorphic response to the MPT probably lessens, as moisture and the extent of past
 832 glaciations is more restricted (Luna et al., 2018; Haselton et al., 2002). Beyond the Central Andes,
 833 fluvial terraces along the Río Deseado (47°S) (Tobal et al., 2021) and Río Santa Cruz (50°S) (Milanez
 834 Fernandes, 2023), draining the Southern Andes in Patagonia also record a period of net incision that
 835 can be tentatively linked to the MPT. On a global scale, a growing number of studies have identified
 836 periods of intensified erosion at this time, for example in the St. Elias mountains, Alaska (Gulick et al.,
 837 2015), Central Appalachia (Del Vecchio et al., 2022), the Rocky Mountains (Pederson and Egholm,
 838 2013) and the European Alps (Haeuselmann et al., 2007; Valla et al., 2011; Sternai et al., 2013). While
 839 it is not possible to discount a tectonic influence on landscape change in the upper Toro basin entirely
 840 due to some chronological ambiguity in the datasets and inherent challenges in deconvolving different
 841 forcing mechanisms, the links between MPT climate and incision, and its expression elsewhere in the
 842 Andes and beyond, is compelling.

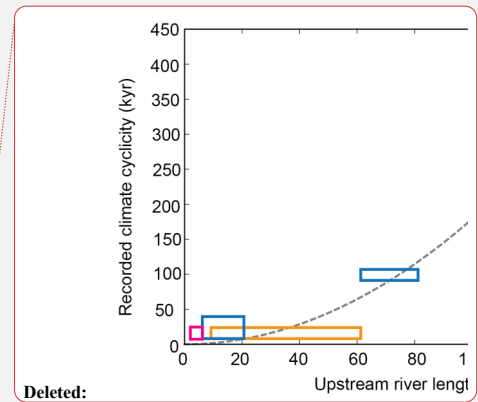
843



844

845 **Figure 9.** Correlation between recorded climate cyclicality and upstream river length recognised in four basins of the Central
 846 Andes: Toro (this study; Tofelde et al., 2017), Humahuaca (Schildgen et al., 2016), Santa María (D'Arcy et al., 2018); Iruya
 847 (Fisher et al., 2016). Unlike the other records of aggradation and incision, the Iruya record is derived from the basin's
 848 sedimentary record and is a paleo-erosion dataset. Adapted from Tofelde et al. (2017). Recorded period: $0.019 \times \text{river length}^2$.

850 **5.4 Climate periodicity and alluvial channel system length**



Deleted: (
 Formatted: Font: (Default) Times New Roman, 9 pt
 Deleted: Fisher et al., 2016; Schildgen et al., 2016; Tofelde et al., 2017; D'Arcy et al. 2018; this study).
 Deleted:

856 Higher frequency climate cycles are recorded in fan generation G2 of the Sierra de Pascha tributaries
857 compared with the mainstem of the basin; the alluvial fans, which appear to record climate cycles with
858 a periodicity of ca. 20 to 40-kyr have an upstream channel length of ~10 km and are positioned ~30 km
859 upstream of the terrace sequence showing 100-kyr climate cyclicity dated by Tofelde et al. (2017). This
860 finding substantiates the theory that the response time of alluvial channel systems to perturbations in
861 climate depends on system length (Paola et al., 1992; Castelltort and Van Den Driessche, 2003; Godard
862 et al., 2013; McNab et al., 2023). Evidence of this relationship, together with the dependency on the
863 square of the system length, was identified in the archive of several sedimentary basins in the Central
864 Andes, although only a single forcing frequency was recorded within each basin (Fig. 9) (Tofelde et al.,
865 2017). Our new data from the Toro Basin provide critical field evidence that multiple climate
866 periodicities can be preserved within the sedimentary record of a single sedimentary basin, with higher
867 forcing frequencies recorded only in the uppermost reaches of the basin.

868

869 6. Conclusions

870

871 The alluvial fan and terrace sequences of the Toro basin present an excellent opportunity to explore (1)
872 how channel responses to external perturbations may or may not propagate downstream, and (2) the
873 differences in landscape response to forcing frequency as a function of stream length. We applied CRN
874 dating to a suite of alluvial fan surfaces to characterise the evolution of the alluvial channel network of
875 the Toro basin over the last one million years. Our key findings are as follows:

876

- 877 1. We identified two generations of fan surfaces (G1 and G2) were identified in the Sierra de
878 Pascha tributary catchments. The G1 fans record CRN exposure (^{10}Be) ages between ca. 800
879 and 500 ka, whereas the G2 fans record surface activity and then abandonment between ca. 100
880 and 20 ka.
- 881 2. The G1 fans capture a significant phase of net incision (~ 200 m) between ca. 800 and 500 ka.
882 The stepwise evacuation of the upper basin coincides with the onset of prolonged and enhanced
883 global glacial cycles following the Mid-Pleistocene Transition (MPT). With several basins in
884 the Central Andes and beyond also registering this phase of incision, we propose that the G1
885 fans are part of a continental scale response to MPT climate change.
- 886 3. The abandonment of the G2 fans is restricted to glacial periods, **possibly** modulated by 21/40-
887 kyr climate cycles; enhanced moisture availability due to an intensified SASM likely amplified
888 channel incision and sediment transport.
- 889 4. Differences in the timing of alluvial fan and fluvial terrace development in the upper and lower
890 Toro basins appear to be associated with how channel length affects fluvial response time to
891 climate forcing as well as local controls on net incision, which facilitates preservation of the
892 geomorphic record of aggradation-incision cycles.

Deleted: mostly

894 5. The new alluvial fan record from the upper Toro Basin, combined with earlier results on fluvial
895 terraces from the lower Toro Basin, provides field evidence for the theoretical predictions of a
896 scaling relationship between climate forcing frequency recorded in sedimentary archives and
897 the system length. We show that multiple climate periodicities can be preserved within the
898 sedimentary record of a single sedimentary basin, with higher forcing frequencies recorded only
899 in the uppermost reaches of the basin. This improved understanding of the role of system length
900 in climate signal propagation is an important step forward in helping us to anticipate the spatial
901 distribution of sedimentary paleoclimate records within landscapes.

902
903

904 7. Code/data availability

905 All data is included as part of the manuscript.

906

907 8. Author contribution

908 Conceptualization: E.N.O, T.F.S, S.T; Sample collection and processing: E.N.O, T.F.S, S.T, H.W.;

909 Visualization: E.N.O with feedback from all authors; Writing & editing: all authors.

910

911 9. Competing interests

912 The authors declare that they have no conflict of interest.

913

914 10. Acknowledgments

915 This work was co-funded by (1) the German Research Foundation (DFG) grant 373/34-1 and the
916 Brandenburg Ministry of Sciences, Research, and Cultural Affairs, within the framework of the
917 International Research Training Group IGK2018 SuRfAce processes, TEctonics and Georesources: The
918 Andean foreland basin of Argentina (StRATEGy) and (2) the European Research Council (ERC) under
919 the European Union's Horizon 2020 Research and Innovation program (ERC Consolidator Grant
920 863490 to T.F.S.). TanDEM-X 12-m resolution digital elevation data were provided by the German
921 Aerospace Center (DLR) through grant DEM_GEOL1915 to T.F. S. We thank Yanina Rojo for logistical
922 support leading up to and during all field work. We also thank Peter van der Beek for assistance during
923 field work.

924

925 11. References

926

927 [Alonso, R.N. Estratigrafía del Cenozoico de la cuenca de Pastos Grandes \(Puna Salteña\) con énfasis](#)
928 [en la Formación. Revista de la Asociación Geológica Argentina, 47\(2\), 189-199.1992.](#)

929 Armitage, J.J., Dunkley Jones, T., Duller, R.A., Whittaker, A.C., Allen, P.A. Temporal buffering of
930 climate-driven sediment flux cycles by transient catchment response. *Earth and Planetary*
931 *Science Letters*, 369–370, 200–210. <https://doi.org/10.1016/j.epsl.2013.03.020>, 2013.

932 Baker, P.A., Rigsby, C.A., Seltzer, G.O., Fritz, S.C., Lowenstein, T.K., Bacher, N.P., Veliz, C. Tropical
933 climate changes at millennial and orbital timescales on the Bolivian Altiplano. *Nature*,
934 409(6821), 698-701. <https://doi.org/10.1038/35055524>, 2001.

935 Baker, P.A., Fritz, S.C. Nature and causes of Quaternary climate variation of tropical South America.
936 *Quaternary Science Reviews*., 124, 31-47. <https://doi.org/10.1016/j.quascirev.2015.06.011>,
937 2015.

938 Berger, A., Li, X.S., Loutre, M.F. Modelling northern hemisphere ice volume over the last 3 Ma.
939 *Quaternary Science Reviews*, 18(1), 1-11. [https://doi.org/10.1016/S0277-3791\(98\)00033-X](https://doi.org/10.1016/S0277-3791(98)00033-X),
940 1999.

941 Berger, A., Loutre, M.F. Insolation values for the climate of the last 10 million years. *Quaternary*
942 *Science Reviews*, 10(4), 297-317. [https://doi.org/10.1016/0277-3791\(91\)90033-Q](https://doi.org/10.1016/0277-3791(91)90033-Q), 1991.

Formatted: Left

- 943 Bernard, T., Sinclair, H.D., Gailleton, B., Mudd, S.M., Ford, M. Lithological control on the post-
 944 orogenic topography and erosion history of the Pyrenees. *Earth and Planetary Science Letters*,
 945 518, 53-66. <https://doi.org/10.1016/j.epsl.2019.04.034>, 2019.
- 946 Blard, P.-H., Braucher, R., Lavé, J., Bourlès, D. Cosmogenic ¹⁰Be production rate calibrated against
 947 ³He in the high Tropical Andes (3800–4900 m, 20–22° S). *Earth and Planetary Science Letters*,
 948 382, 140–149. <https://doi.org/10.1016/j.epsl.2013.09.010>, 2013.
- 949 Bobst, A.L., Lowenstein, T.K., Jordan, T.E., Godfrey, L.V., Ku, T.L., Luo, S. A 106 ka paleoclimate
 950 record from drill core of the Salar de Atacama, northern Chile. *Palaeogeography,*
 951 *Palaeoclimatology, Palaeoecology*, 173(1-2), 21-42. [https://doi.org/10.1016/S0031-](https://doi.org/10.1016/S0031-0182(01)00308-X)
 952 [0182\(01\)00308-X](https://doi.org/10.1016/S0031-0182(01)00308-X), 2001.
- 953 Bonorino, G.G., Abascal, L. Drainage and base-level adjustments during evolution of a late Pleistocene
 954 piggyback basin, Eastern Cordillera, Central Andes of northwestern Argentina. *Bulletin*,
 955 124(11-12), 1858-1870. <https://doi.org/10.1130/B30395.1>, 2012.
- 956 Bookhagen, B., Strecker, M.R. Orographic barriers, high-resolution TRMM rainfall, and relief
 957 variations along the eastern Andes. *Geophysical Research Letters*, 35.
 958 <https://doi.org/10.1029/2007GL032011>, 2008.
- 959 [Bridgland, D., Westaway, R. Climatically controlled river terrace staircases: a worldwide Quaternary
 960 phenomenon. *Geomorphology*, 98\(3-4\), 285-315,
 961 <https://doi.org/10.1016/j.geomorph.2006.12.032>, 2008.](https://doi.org/10.1016/j.geomorph.2006.12.032)
- 962 Brocard, G., Willenbring, J., Suski, B., Audra, P., Authemayou, C., Cosenza-Murales, B., Morán-Ical,
 963 S., Demory, F., Rochette, P., Vennemann, T., Holliger, K. Rate and processes of river network
 964 rearrangement during incipient faulting: The case of the Cahabón River, Guatemala. *American*
 965 *Journal of Science*, 312(5), 449-507, <https://doi.org/10.2475/05.2012.01>, 2012.
- 966 Broccoli, A.J., Dahl, K.A., Stouffer, R.J. Response of the ITCZ to Northern Hemisphere cooling.
 967 *Geophysical Research Letters*, 33(1). <https://doi.org/10.1029/2005GL024546>, 2006.
- 968 Brooke, S.A., Whittaker, A.C., Armitage, J.J., D'Arcy, M., Watkins, S.E. Quantifying sediment
 969 transport dynamics on alluvial fans from spatial and temporal changes in grain size, Death
 970 Valley, California. *Journal of Geophysical Research: Earth Surface*, 123(8), 2039-2067.
 971 <https://doi.org/10.1029/2018JF004622>, 2018.
- 972 Bufe, A., Burbank, D.W., Liu, L., Bookhagen, B., Qin, J., Chen, J., Li, T., Thompson Jobe, J.A., Yang,
 973 H. Variations of lateral bedrock erosion rates control planation of uplifting folds in the foreland
 974 of the Tian Shan, NW China. *Journal of Geophysical Research: Earth Surface*, 122(12), 2431-
 975 2467. <https://doi.org/10.1002/2016JF004099>, 2017.
- 976 Buter, A., Heckmann, T., Filisetti, L., Savi, S., Mao, L., Gems, B., Comiti, F. Effects of catchment
 977 characteristics and hydro-meteorological scenarios on sediment connectivity in glacierised
 978 catchments. *Geomorphology*, 402, 108128. <https://doi.org/10.1016/j.geomorph.2022.108128>,
 979 2022.
- 980 Castellort, S., Van Den Driessche, J. How plausible are high-frequency sediment supply-driven cycles
 981 in the stratigraphic record? *Sedimentary Geology*, 157, 3–13. [https://doi.org/10.1016/S0037-](https://doi.org/10.1016/S0037-0738(03)00066-6)
 982 [0738\(03\)00066-6](https://doi.org/10.1016/S0037-0738(03)00066-6), 2003.
- 983 Castino, F., Bookhagen, B., Strecker, M.R. Rainfall variability and trends of the past six decades (1950–
 984 2014) in the subtropical NW Argentine Andes. *Climate Dynamics*, 48, 1049-1067.
 985 <https://doi.org/10.1007/s00382-016-3127-2>, 2017.
- 986 Cesta, J.M., Ward, D.J. Timing and nature of alluvial fan development along the Chajnantor Plateau,
 987 northern Chile. *Geomorphology*, 273, 412–427.
 988 <https://doi.org/10.1016/j.geomorph.2016.09.003>, 2016.
- 989 Clarke, L., Quine, T.A., Nicholas, A. An experimental investigation of autogenic behaviour during
 990 alluvial fan evolution. *Geomorphology*, 115(3-4), 278-285.
 991 <https://doi.org/10.1016/j.geomorph.2009.06.033>, 2010.
- 992 Counts, R.C., Murari, M.K., Owen, L.A., Mahan, S.A., Greenan, M. Late Quaternary
 993 chronostratigraphic framework of terraces and alluvium along the lower Ohio River,
 994 southwestern Indiana and western Kentucky, USA. *Quaternary Science Reviews*, 110, 72-91.
 995 <https://doi.org/10.1016/j.quascirev.2014.11.011>, 2015.
- 996 Crivellari, S., Chiessi, C.M., Kuhnert, H., Häggi, C., da Costa Portillo-Ramos, R., Zeng, J.Y., Zhang,
 997 Y., Schefuß, E., Mollenhauer, G., Hefter, J., Alexandre, F. Increased Amazon freshwater

Formatted: Font: (Default) Times New Roman, 11 pt, Font colour: Auto

Formatted: Left

Formatted: Font: (Default) Times New Roman, 11 pt, Not Italic, Font colour: Auto

Formatted: Font: (Default) Times New Roman, 11 pt, Font colour: Auto

Formatted: Font: (Default) Times New Roman, 11 pt, Not Italic, Font colour: Auto

Formatted: Font: (Default) Times New Roman, 11 pt, Font colour: Auto

Formatted: Font: (Default) Times New Roman

Formatted: Font: (Default) Times New Roman

Formatted: Font: (Default) Times New Roman

998 discharge during late Heinrich Stadial 1. *Quaternary Science Reviews*, 181, 144-155.
999 <https://doi.org/10.1016/j.quascirev.2017.12.005>, 2018.

1000 D’Arcy, M.K., Schildgen, T.F., Strecker, M.R., Wittmann, H., Duesing, W., Mey, J., Tofelde, S.,
1001 Weissmann, P., Alonso, R.N. Timing of past glaciation at the Sierra de Aconquija, northwestern
1002 Argentina, and throughout the Central Andes. *Quaternary Science Reviews*, 204, 37–57.
1003 <https://doi.org/10.1016/j.quascirev.2018.11.022>, 2019a.

1004 D’Arcy, M.K., Schildgen, T.F., Turowski, J.M., Dinezio, P. Inferring the timing of abandonment of
1005 aggraded alluvial surfaces dated with cosmogenic nuclides. *Earth Surface Dynamics*, 7, 755–
1006 771. <https://doi.org/10.5194/esurf-7-755-2019>, 2019b.

1007 D’Arcy, M., Schildgen, T.F., Tofelde, S., Strecker, M.R., Wittmann, H., Düsing, W., Weissmann, P.
1008 and Roda-Boluda, D.C. Catchment-alluvial fan systems record > 200 ka of millennial-scale
1009 climate changes in the subtropical Andes. *EGU General Assembly Conference Abstracts*.
1010 <https://ui.adsabs.harvard.edu/abs/2018EGUGA..20.4710D/abstract>, 2018.

1011 DeCelles, P.G., Carrapa, B., Horton, B.K., Gehrels, G.E. Cenozoic foreland basin system in the central
1012 Andes of northwestern Argentina: Implications for Andean geodynamics and modes of
1013 deformation. *Tectonics*, 30(6). <https://doi.org/10.1029/2011TC002948>, 2011.

1014 Del Vecchio, J., DiBiase, R.A., Corbett, L.B., Bierman, P.R., Caffee, M.W., Ivory, S.J. Increased
1015 erosion rates following the onset of Pleistocene periglaciation at Bear Meadows, Pennsylvania,
1016 USA. *Geophysical Research Letters*, 49(4), p.e2021GL096739.
1017 <https://doi.org/10.1029/2021GL096739>, 2022.

1018 Dey, S., Thiede, R.C., Schildgen, T.F., Wittmann, H., Bookhagen, B., Scherler, D., Jain, V., Strecker,
1019 M.R. Climate-driven sediment aggradation and incision since the late Pleistocene in the NW
1020 Himalaya, India. *Earth and Planetary Science Letters*, 449, 321–331.
1021 <https://doi.org/10.1016/j.epsl.2016.05.050>, 2016.

1022 Dortch, J.M., Tomkins, M.D., Saha, S., Murari, M.K., Schoenbohm, L.M., Curl, D. A tool for the ages:
1023 The Probabilistic Cosmogenic Age Analysis Tool (P-CAAT). *Quaternary Geochronology*, 71,
1024 101323. <https://doi.org/10.1016/j.quageo.2022.101323>, 2022.

1025 Dühnforth, M., Densmore, A.L., Ivy-Ochs, S., Allen, P., Kubik, P.W. Early to Late Pleistocene history
1026 of debris-flow fan evolution in western Death Valley (California) using cosmogenic ¹⁰Be and
1027 ²⁶Al. *Geomorphology*, 281, 53–65. <https://doi.org/10.1016/j.geomorph.2016.12.020>, 2017.

1028 Dühnforth, M., Densmore, A.L., Ivy-Ochs, S., Allen, P.A., Kubik, P.W. Timing and patterns of debris
1029 flow deposition on Shepherd and Symmes creek fans, Owens Valley, California, deduced from
1030 cosmogenic ¹⁰Be. *Journal of Geophysical Research: Earth Surface*, 112.
1031 <https://doi.org/10.1029/2006JF000562>, 2007.

1032 Dunai, T.J., López, G.A.G., Juez-Larré, J. Oligocene–Miocene age of aridity in the Atacama Desert
1033 revealed by exposure dating of erosion-sensitive landforms. *Geology*, 33(4), 321-324.
1034 <https://doi.org/10.1130/G21184.1>, 2005.

1035 Fernandes, V.M., Schildgen, T., Ruby, A., Wittmann-Oelze, H., McNab, F. Pleistocene Landscape
1036 Evolution in Southern Patagonia: A Record of Regional Incision from ¹⁰Be Dating of Fluvial
1037 Terraces (No. EGU23-15938). *Copernicus Meetings*. <https://doi.org/10.5194/egusphere-egu23-15938>, 2023.

1039 Fisher, G.B., Luna, L.V., Amidon, W.H., Burbank, D.W., de Boer, B., Stap, L.B., Bookhagen, B.,
1040 Godard, V., Oskin, M.E., Alonso, R.N., and Tuenter, E. Milankovitch-paced erosion in the
1041 southern Central Andes. *Nature Communications*, 14(1), 424 <https://doi.org/10.1038/s41467-023-36022-0>, 2023.

1043 Fritz, S.C., Baker, P.A., Ekdahl, E., Seltzer, G.O., Stevens, L.R. Millennial-scale climate variability
1044 during the Last Glacial period in the tropical Andes. *Quaternary Science Reviews*, 29(7-8),
1045 1017-1024. <https://doi.org/10.1016/j.quascirev.2010.01.001>, 2010.

1046 Fritz, S.C., Baker, P.A., Seltzer, G.O., Ballantyne, A., Tapia, P., Cheng, H., Edwards, R.L. Quaternary
1047 glaciation and hydrologic variation in the South American tropics as reconstructed from the
1048 Lake Titicaca drilling project. *Quaternary Research*, 68(3), 410-420.
1049 <https://doi.org/10.1016/j.yqres.2007.07.008>, 2007.

1050 Fritz, S.C., Baker, P.A., Lowenstein, T.K., Seltzer, G.O., Rigsby, C.A., Dwyer, G.S., Tapia, P.M.,
1051 Arnold, K.K., Ku, T.L., Luo, S. Hydrologic variation during the last 170,000 years in the

1052 southern hemisphere tropics of South America. *Quaternary Research*, 61(1), 95-104.
1053 <https://doi.org/10.1016/j.yqres.2003.08.007>, 2004.

1054 Fryirs, K.A., Brierley, G.J., Preston, N.J., Kasai, M. Buffers, barriers and blankets: The (dis)
1055 connectivity of catchment-scale sediment cascades. *Catena*, 70(1), 49-67.
1056 <https://doi.org/10.1016/j.catena.2006.07.007>, 2007.

1057 Ganev, P.N., Dolan, J.F., Frankel, K.L., Finkel, R.C. Rates of extension along the Fish Lake Valley
1058 fault and transtensional deformation in the Eastern California shear zone–Walker Lane belt.
1059 *Lithosphere*, 2(1), 33-49. <https://doi.org/10.1130/L51.1>, 2010.

1060 García, V.H., Hongn, F., Cristallini, E.O. Late Miocene to recent morphotectonic evolution and
1061 potential seismic hazard of the northern Lerma valley: clues from Lomas de Medeiros,
1062 Cordillera Oriental, NW Argentina. *Tectonophysics*, 608, 1238-1253.
1063 <https://doi.org/10.1016/j.tecto.2013.06.021>, 2013.

1064 Godard, V., Tucker, G.E., Burch Fisher, G., Burbank, D.W., Bookhagen, B. Frequency-dependent
1065 landscape response to climatic forcing. *Geophysical Research Letters*, 40, 859–863.
1066 <https://doi.org/10.1002/grl.50253>, 2013.

1067 Godfrey, L.V., Jordan, T.E., Lowenstein, T.K., Alonso, R.L. Stable isotope constraints on the transport
1068 of water to the Andes between 22 and 26 S during the last glacial cycle. *Palaeogeography*,
1069 *Palaeoclimatology*, *Palaeoecology*, 194(1-3), 299-317. [https://doi.org/10.1016/S0031-](https://doi.org/10.1016/S0031-0182(03)00283-9)
1070 [0182\(03\)00283-9](https://doi.org/10.1016/S0031-0182(03)00283-9), 2003.

1071 Gosling, W.D., Bush, M.B., Hanselman, J.A., Chepstow-Lusty, A. Glacial-interglacial changes in
1072 moisture balance and the impact on vegetation in the southern hemisphere tropical Andes
1073 (Bolivia/Peru). *Palaeogeography*, *Palaeoclimatology*, *Palaeoecology*, 259(1), 35-50.
1074 <https://doi.org/10.1016/j.palaeo.2007.02.050>, 2008.

1075 Gray, H.J., Owen, L.A., Dietsch, C., Beck, R.A., Caffee, M.A., Finkel, R.C., Mahan, S.A. Quaternary
1076 landscape development, alluvial fan chronology and erosion of the Mecca Hills at the southern
1077 end of the San Andreas fault zone. *Quaternary Science Reviews*, 105, 66-85.
1078 <https://doi.org/10.1016/j.quascirev.2014.09.009>, 2014.

1079 Guarnieri, P., Pirrotta, C. The response of drainage basins to the late Quaternary tectonics in the Sicilian
1080 side of the Messina Strait (NE Sicily). *Geomorphology*, 95(3-4), 260-273.
1081 <https://doi.org/10.1016/j.geomorph.2007.06.013>, 2008.

1082 Gulick, S.P., Jaeger, J.M., Mix, A.C., Asahi, H., Bahlburg, H., Belanger, C.L., Berbel, G.B., Childress,
1083 L., Cowan, E., Drab, L., Forwick, M. Mid-Pleistocene climate transition drives net mass loss
1084 from rapidly uplifting St. Elias Mountains, Alaska. *Proceedings of the National Academy of*
1085 *Sciences*, 112(49), 15042-15047. <https://doi.org/10.1073/pnas.1512549112>, 2015.

1086 Haeuselmann, P., Granger, D.E., Jeannin, P.Y., Lauritzen, S.E. Abrupt glacial valley incision at 0.8 Ma
1087 dated from cave deposits in Switzerland. *Geology*, 35(2), 143-146.
1088 <https://doi.org/10.1130/G23094A>, 2007.

1089 Hain, M.P., Strecker, M.R., Bookhagen, B., Alonso, R.N., Pingel, H., Schmitt, A.K. Neogene to
1090 Quaternary broken foreland formation and sedimentation dynamics in the Andes of NW
1091 Argentina (25 S). *Tectonics*, 30(2). <https://doi.org/10.1029/2010TC002703>, 2011.

1092 Harvey, A.M. The coupling status of alluvial fans and debris cones: a review and synthesis. *Earth*
1093 *Surface Processes and Landforms*, 37(1), 64-76. <https://doi.org/10.1002/esp.2213>, 2012.

1094 Harvey, A.M., Silva, P.G., Mather, A.E., Goy, J.L., Stokes, M., Zazo, C. The impact of Quaternary sea-
1095 level and climatic change on coastal alluvial fans in the Cabo de Gata ranges, southeast Spain.
1096 *Geomorphology*, 28(1-2), 1-22 [https://doi.org/10.1016/S0169-555X\(98\)00100-7](https://doi.org/10.1016/S0169-555X(98)00100-7), 1999.

1097 Haselton, K., Hilley, G., Strecker, M.R. Average Pleistocene climatic patterns in the southern central
1098 Andes: Controls on mountain glaciation and paleoclimate implications. *The Journal of*
1099 *Geology*, 110(2), 211-226. 2002.

1100 Hedrick, K., Owen, L.A., Rockwell, T.K., Meigs, A., Costa, C., Caffee, M.W., Masana, E., Ahumada,
1101 E. Timing and nature of alluvial fan and strath terrace formation in the Eastern Precordillera of
1102 Argentina. *Quaternary Science Reviews*, 80, 143–168
1103 <https://doi.org/10.1016/j.quascirev.2013.05.004>, 2013.

1104 Hidy, A.J., Gosse, J.C., Pederson, J.L., Mattern, J.P., Finkel, R.C. A geologically constrained Monte
1105 Carlo approach to modeling exposure ages from profiles of cosmogenic nuclides: An example

1106 from Lees Ferry, Arizona. *Geochemistry Geophysics Geosystems*, 11, Q0AA10.
1107 <https://doi.org/10.1029/2010GC003084>, 2010.

1108 Hilley, G.E., Strecker, M.R. Processes of oscillatory basin filling and excavation in a tectonically active
1109 orogen: Quebrada del Toro Basin, NW Argentina. *Bulletin of the Geological Society of*
1110 *America*, 117, 887–901. <https://doi.org/10.1130/B25602.1>, 2005.

1111 Howard, A.D. Equilibrium and time scales in geomorphology: Application to sand-bed alluvial streams.
1112 *Earth Surface Processes and Landforms*, 7(4), pp.303-325.
1113 <https://doi.org/10.1002/esp.3290070403>, 1982.

1114 Hughes, P.D. Geomorphology and Quaternary stratigraphy: The roles of morpho-, litho-, and
1115 allostratigraphy. *Geomorphology*, 123, 189–199.
1116 <https://doi.org/10.1016/j.geomorph.2010.07.025>, 2010.

1117 Imbrie, John., McIntyre, Andrew. SST vs time for core V25-21 (specmap.059). PANGAEA., 2006.

1118 Kelly, M.A., Lowell, T. V., Applegate, P.J., Phillips, F.M., Schaefer, J.M., Smith, C.A., Kim, H.,
1119 Leonard, K.C., Hudson, A.M. A locally calibrated, late glacial ¹⁰Be production rate from a low-
1120 latitude, high-altitude site in the Peruvian Andes. *Quaternary Geochronology*, 26, 70–85.
1121 <https://doi.org/10.1016/j.quageo.2013.10.007>, 2015.

1122 Kleinert, K., Strecker, M.R. Climate change in response to orographic barrier uplift: Paleosol and stable
1123 isotope evidence from the late Neogene Santa Maria basin, northwestern Argentina. *Geological*
1124 *Society of America Bulletin*, 113(6), 728-742. [https://doi.org/10.1130/0016-7606\(2001\)113<0728:CCIRTO>2.0.CO;2](https://doi.org/10.1130/0016-7606(2001)113<0728:CCIRTO>2.0.CO;2), 2001.

1126 Kober, F., Zeilinger, G., Ivy-Ochs, S., Dolati, A., Smit, J., Kubik, P.W. Climatic and tectonic control
1127 on fluvial and alluvial fan sequence formation in the Central Makran Range, SE-Iran. *Global*
1128 *and Planetary Change*, 111, 133-149. <https://doi.org/10.1016/j.gloplacha.2013.09.003>, 2013.

1129 Lal, D. Cosmic ray labeling of erosion surfaces: in situ nuclide production rates and erosion models.
1130 *Earth and Planetary Science Letters*, 104, 424–439. [https://doi.org/10.1016/0012-821X\(91\)90220-C](https://doi.org/10.1016/0012-821X(91)90220-C), 1991.

1132 Lifton, N., Sato, T., Dunai, T.J. Scaling in situ cosmogenic nuclide production rates using analytical
1133 approximations to atmospheric cosmic-ray fluxes. *Earth and Planetary Science Letters*, 386,
1134 149–160. <https://doi.org/10.1016/j.epsl.2013.10.052>, 2014.

1135 Lisiecki, L.E., Raymo, M.E. Diachronous benthic $\delta^{18}O$ responses during late Pleistocene terminations.
1136 *Paleoceanography*, 24(3). <https://doi.org/10.1029/2009PA001732>, 2009.

1137 Luna, L. V., Bookhagen, B., Niedermann, S., Rugel, G., Scharf, A., Merchel, S. Glacial chronology and
1138 production rate cross-calibration of five cosmogenic nuclide and mineral systems from the
1139 southern Central Andean Plateau. *Earth and Planetary Science Letters*, 500, 242–253.
1140 <https://doi.org/10.1016/j.epsl.2018.07.034>, 2018.

1141 Ma, Y., Stuart, F.M. The use of in-situ cosmogenic ²¹Ne in studies on long-term landscape development.
1142 *Acta Geochimica*, 37, 310-322. <https://doi.org/10.1007/s11631-017-0216-9>, 2018.

1143 Mackin, J. Concept of the graded river. *Geological Society of America Bulletin*, 59(5), 463-512, 1948.

1144 Malamud, B.D., Jordan, T.E., Alonso, R.A., Gallardo, E.F., Gonzalez, R.E., Kelley, S.A. Pleistocene
1145 Lake Lerma, Salta Province, NW Argentina. In XIII Congreso Geológico Argentino y III
1146 Congreso de Exploración de Hidrocarburos, Vol. 1, 103-114, 1996.

1147 Marrett, R., Strecker, M.R. Response of intracontinental deformation in the central Andes to late
1148 Cenozoic reorganization of South American Plate motions. *Tectonics*, 19(3), 452-467.
1149 <https://doi.org/10.1029/1999TC001102>, 2000.

1150 Marrett, R.A., Allmendinger, R.W., Alonso, R.N., Drake, R.E. Late Cenozoic tectonic evolution of the
1151 Puna Plateau and adjacent foreland, northwestern Argentine Andes. *Journal of South American*
1152 *Earth Sciences*, 7(2), 179-207. [https://doi.org/10.1016/0895-9811\(94\)90007-8](https://doi.org/10.1016/0895-9811(94)90007-8), 1994.

1153 Martin, L.C.P., Blard, P.-H., Balco, G., Lavé, J., Delunel, R., Lifton, N., Laurent, V. The CREp program
1154 and the ICE-D production rate calibration database: A fully parameterizable and updated online
1155 tool to compute cosmic-ray exposure ages. *Quaternary Geochronology*, 38, 25–49.
1156 <https://doi.org/10.1016/j.quageo.2016.11.006>, 2017.

1157 Martin, L.C.P., Blard, P.-H., Lavé, J., Braucher, R., Lupker, M., Condom, T., Charreau, J., Mariotti, V.,
1158 ASTER Team, Davy, E. In situ cosmogenic ¹⁰Be production rate in the High Tropical Andes.
1159 *Quaternary Geochronology*, 30, 54–68. <https://doi.org/10.1016/j.quageo.2015.06.012>, 2015.

1160 Martin, L.C., Blard, P.H., Lavé, J., Condom, T., Prémaillon, M., Jomelli, V., Brunstein, D., Lupker, M.,
1161 Charreau, J., Mariotti, V., Tibari, B. Lake Tauca highstand (Heinrich Stadial 1a) driven by a
1162 southward shift of the Bolivian High. *Science Advances*, 4(8),
1163 <https://doi.org/10.1126/sciadv.aar2514>, 2018.

1164 Martini, M.A., Kaplan, M.R., Strelin, J.A., Astini, R.A., Schaefer, J.M., Caffee, M.W., Schwartz, R.
1165 Late Pleistocene glacial fluctuations in Cordillera oriental, subtropical Andes. *Quaternary*
1166 *Science Reviews*, 171, 245-259. <https://doi.org/10.1016/j.quascirev.2017.06.033>, 2017.

1167 Mather, A.E., Stokes, M., Whitfield, E. River terraces and alluvial fans: The case for an integrated
1168 Quaternary fluvial archive. *Quaternary Science Reviews* 166, 74-90,
1169 <https://doi.org/10.1016/j.quascirev.2016.09.022>, 2017.

1170 Mazzuoli, R., Vezzoli, L., Omarini, R., Acocella, V., Gioncada, A., Matteini, M., Dini, A., Guillou, H.,
1171 Hauser, N., Uttini, A., Scaillet, S. Miocene magmatism and tectonics of the easternmost sector
1172 of the Calama–Olacapato–El Toro fault system in Central Andes at~ 24 S: Insights into the
1173 evolution of the Eastern Cordillera. *GSA Bulletin* 120(11-12), 1493-1517,
1174 <https://doi.org/10.1130/B26109.1>, 2008.

1175 McFadden, L.D., Ritter, J.B., Wells, S.G. Use of Multiparameter Relative-Age Methods for Age
1176 Estimation and Correlation of Alluvial Fan Surfaces on a Desert Piedmont, Eastern Mojave
1177 Desert, California. *Quaternary Research* 32, 276–290, [https://doi.org/10.1016/0033-5894\(89\)90094-X](https://doi.org/10.1016/0033-5894(89)90094-X), 1989.

1179 McNab, F., Schildgen, T.F., Turowski, J.M., Wickert, A.D. Diverse responses of alluvial rivers to
1180 periodic environmental change. *Geophysical Research Letters* 50(10), e2023GL103075,
1181 <https://doi.org/10.1029/2023GL103075>, 2023.

1182 Mescolotti, P.C., do Nascimento Pupim, F., Ladeira, F.S.B., Sawakuchi, A.O., Santa Catharina, A.,
1183 Assine, M.L. Fluvial aggradation and incision in the Brazilian tropical semi-arid: Climate-
1184 controlled landscape evolution of the São Francisco River. *Quaternary Science Reviews* 263,
1185 106977, <https://doi.org/10.1016/j.quascirev.2021.106977>, 2021.

1186 Messager, G., Huyghe, D., Bonnel, C., Nivière, B., Fasentieux, B. The Neogene to Quaternary evolution
1187 of the Neuquén Andes broken foreland forced by tectonic, climatic and surface processes
1188 (southern Central Andes). *Journal of South American Earth Sciences*, 131, 104620,
1189 <https://doi.org/10.1016/j.jsames.2023.104620>.

1190 Mey, J., D'Arcy, M.K., Schildgen, T.F., Egholm, D.L., Wittmann, H., Strecker, M.R. Temperature and
1191 precipitation in the southern Central Andes during the last glacial maximum, Heinrich Stadial
1192 1, and the Younger Dryas. *Quaternary Science Reviews* 248, 106592,
1193 <https://doi.org/10.1016/j.quascirev.2020.106592>, 2020.

1194 Mosblech, N.A., Bush, M.B., Gosling, W.D., Hodell, D., Thomas, L., Van Calsteren, P., Correa-Metrio,
1195 A., Valencia, B.G., Curtis, J., Van Woesik, R. North Atlantic forcing of Amazonian
1196 precipitation during the last ice age. *Nature Geoscience* 5(11), 817-820,
1197 <https://doi.org/10.1038/ngeo1588>, 2012.

1198 Mouchéné, M., van der Beek, P., Carretier, S., Mouthereau, F. Autogenic versus allogenic controls on
1199 the evolution of a coupled fluvial megafan–mountainous catchment system: numerical
1200 modelling and comparison with the Lannemezan megafan system (northern Pyrenees, France).
1201 *Earth Surface Dynamics* 5(1), 125-143, <https://doi.org/10.5194/esurf-5-125-2017>, 2017.

1202 Mouslopoulou, V., Begg, J., Fülling, A., Moraetis, D., Partsinevelos, P., Oncken, O. Distinct phases of
1203 eustatic and tectonic forcing for late Quaternary landscape evolution in southwest Crete,
1204 Greece. *Earth Surface Dynamics* 5(3), 511-527, <https://doi.org/10.5194/esurf-5-511-2017>,
1205 2017.

1206 Nicholas, A.P., Quine, T.A. Modeling alluvial landform change in the absence of external
1207 environmental forcing. *Geology* 35(6), 527-530, <https://doi.org/10.1130/G23377A.1>, 2007.

1208 Nishiizumi, K., Winterer, E.L., Kohl, C.P., Klein, J., Middleton, R., Lal, D., Arnold, J.R. Cosmic ray
1209 production rates of ¹⁰Be and ²⁶Al in quartz from glacially polished rocks. *Journal of Geophysical*
1210 *Research* 94, 17907, <https://doi.org/10.1029/JB094iB12p17907>, 1989.

1211 Novello, V.F., Cruz, F.W., Vuille, M., Strikis, N.M., Edwards, R.L., Cheng, H., Emerick, S., De Paula,
1212 M.S., Li, X., Barreto, E.D.S., Karmann, I. A high-resolution history of the South American
1213 Monsoon from Last Glacial Maximum to the Holocene. *Scientific Reports* 7(1), 44267,
1214 <https://doi.org/10.1038/srep44267>, 2017.

Formatted: Font: (Default) Times New Roman, 11 pt, Font colour: Auto

Formatted: Font: (Default) Times New Roman, 11 pt, Not Italic, Font colour: Auto

Formatted: Font: (Default) Times New Roman, 11 pt, Font colour: Auto

Formatted: Font: (Default) Times New Roman, 11 pt, Not Italic, Font colour: Auto

Formatted: Font: (Default) Times New Roman, 11 pt, Font colour: Auto

Formatted: Font: (Default) Times New Roman

Formatted: Font: (Default) Times New Roman

- 1215 Orr, E.N., Owen, L.A., Saha, S., Caffee, M.W. Climate-driven late Quaternary fan surface abandonment
 1216 in the NW Himalaya. In: *Untangling the Quaternary Period—A Legacy of Stephen C. Porter*.
 1217 Geological Society of America, 63–80. [https://doi.org/10.1130/2020.2548\(04\)](https://doi.org/10.1130/2020.2548(04)), 2021.
- 1218 Owen, L.A., Clemmens, S.J., Finkel, R.C., Gray, H. Late Quaternary alluvial fans at the eastern end of
 1219 the San Bernardino Mountains, Southern California. *Quaternary Science Reviews*, 87, 114–
 1220 134. <https://doi.org/10.1016/j.quascirev.2014.01.003>, 2014.
- 1221 Paola, C., Heller, P.L., Angevine, C.L. The large-scale dynamics of grain-size variation in alluvial
 1222 basins, 1: theory. *Basin Research*, 4, 73–90. [https://doi.org/10.1111/j.1365-
 1223 2117.1992.tb00145.x.1992](https://doi.org/10.1111/j.1365-2117.1992.tb00145.x.1992).
- 1224 [Pearson, D.M., Kapp, P., DeCelles, P.G., Reiners, P.W., Gehrels, G.E., Ducea, M.N., Pullen, A.](https://doi.org/10.1130/GES00923.1)
 1225 [Influence of pre-Andean crustal structure on Cenozoic thrust belt kinematics and shortening](https://doi.org/10.1130/GES00923.1)
 1226 [magnitude: Northwestern Argentina. *Geosphere*, 9\(6\), 1766–1782. 2013.](https://doi.org/10.1130/GES00923.1)
 1227 <https://doi.org/10.1130/GES00923.1>
- 1228 Pedersen, V.K., Egholm, D.L. Glaciations in response to climate variations preconditioned by evolving
 1229 topography. *Nature*, 493(7431), 206–210. <https://doi.org/10.1038/nature11786>, 2013.
- 1230 Peri, V.G., Haghipour, N., Christl, M., Terrizzano, C., Kaveh-Firouz, A., Leiva, M.F., Pérez, P., Yamin,
 1231 M., Barcelona, H., Burg, J.P. Quaternary landscape evolution in the Western Argentine
 1232 Precordillera constrained by ¹⁰Be cosmogenic dating. *Geomorphology* 396.
 1233 <https://doi.org/10.1016/j.geomorph.2021.107984>, 2022.
- 1234 Perron, J.T., Royden, L. An integral approach to bedrock river profile analysis. *Earth Surface Processes*
 1235 *and Landforms*, 38(6), 570–576. <https://doi.org/10.1002/esp.3302>, 2013.
- 1236 Pingel, H., Strecker, M.R., Mulch, A., Alonso, R.N., Cottle, J., Rohrmann, A. Late Cenozoic
 1237 topographic evolution of the Eastern Cordillera and Puna Plateau margin in the southern Central
 1238 Andes (NW Argentina). *Earth and Planetary Science Letters* 535, 116112.
 1239 <https://doi.org/10.1016/j.epsl.2020.116112>, 2020.
- 1240 Pingel, H., Alonso, R.N., Altenberger, U., Cottle, J., Strecker, M.R. Miocene to Quaternary basin
 1241 evolution at the southeastern Andean Plateau (Puna) margin (ca. 24°S lat, Northwestern
 1242 Argentina). *Basin Research* 31, 808–826. <https://doi.org/10.1111/bre.12346>, 2019a.
- 1243 Pingel, H., Schildgen, T., Strecker, M.R., Wittmann, H. Pliocene–Pleistocene orographic control on
 1244 denudation in northwest Argentina. *Geology* 47, 359–362. <https://doi.org/10.1130/G45800.1>,
 1245 2019b.
- 1246 Pingel, H., Mulch, A., Alonso, R.N., Cottle, J., Hynek, S.A., Poletti, J., Rohrmann, A., Schmitt, A.K.,
 1247 Stockli, D.F. and Strecker, M.R. Surface uplift and convective rainfall along the southern
 1248 Central Andes (Angastaco Basin, NW Argentina). *Earth and Planetary Science Letters*, 440,
 1249 33–42. <https://doi.org/10.1016/j.epsl.2016.02.009>, 2016.
- 1250 Pingel, H., Strecker, M.R., Alonso, R.N., Schmitt, A.K. Neotectonic basin and landscape evolution in
 1251 the Eastern Cordillera of NW Argentina, Humahuaca Basin (~ 24 S). *Basin Research*, 25(5),
 1252 554–573. <https://doi.org/10.1111/bre.12016>, 2013.
- 1253 Placzek, C., Quade, J., Patchett, P.J. Geochronology and stratigraphy of late Pleistocene lake cycles on
 1254 the southern Bolivian Altiplano: implications for causes of tropical climate change. *Geological*
 1255 *Society of America Bulletin*, 118(5–6), 515–532. <https://doi.org/10.1130/B25770.1>, 2006.
- 1256 Prush, V.B., Oskin, M.E. A mechanistic erosion model for cosmogenic nuclide inheritance in single-
 1257 clast exposure ages. *Earth and Planetary Science Letters* 535, 116066.
 1258 <https://doi.org/10.1016/j.epsl.2020.116066>, 2020.
- 1259 Ratnayaka, K., Hetzel, R., Hornung, J., Hampel, A., Hinderer, M., Frechen, M. Postglacial alluvial fan
 1260 dynamics in the Cordillera Oriental, Peru, and palaeoclimatic implications. *Quaternary*
 1261 *Research*, 91, 431–449. <https://doi.org/10.1017/qua.2018.106>, 2019.
- 1262 Robinson, R.A.J., Spencer, J.Q.G., Strecker, M.R., Richter, A., Alonso, R.N. Luminescence dating of
 1263 alluvial fans in intramontane basins of NW Argentina. In: Harvey, A.M. et. al, eds. *Alluvial*
 1264 *Fans: Geomorphology, Sedimentology, Dynamics*. Geological Society. Special Publication
 1265 251, 153–168. 2005.
- 1266 Rohais, S., Bonnet, S. and Eschard, R. Sedimentary record of tectonic and climatic erosional
 1267 perturbations in an experimental coupled catchment–fan system. *Basin Research*, 24(2), 198–
 1268 212. <https://doi.org/10.1111/j.1365-2117.2011.00520.x>, 2012.

Formatted: Left

Deleted: Robledo Juan M., Luisa M. Anzótegui, Olga G. Martínez, Ricardo N. Alonso. Flora and insect trace fossils from the Mio-Pliocene Quebrada del Toro locality (Governador Solá, Salta, Argentina). *Journal of South American Earth Sciences*, Volume 100, June 2020, 102544. <https://doi.org/10.1016/j.jsames.2020.102544>, 2020. ¶

1275 Savi, S., Tofelde, S., Wickert, A.D., Bufo, A., Schildgen, T.F., Strecker, M.R. Interactions between
1276 main channels and tributary alluvial fans: channel adjustments and sediment-signal
1277 propagation. *Earth Surface Dynamics*, 8(2), 303-322. [https://doi.org/10.5194/esurf-8-303-](https://doi.org/10.5194/esurf-8-303-2020)
1278 [2020](https://doi.org/10.5194/esurf-8-303-2020), 2020.

1279 Savi, S., Schildgen, T.F., Tofelde, S., Wittmann, H., Scherler, D., Mey, J., Alonso, R.N., Strecker, M.R.
1280 Climatic controls on debris-flow activity and sediment aggradation: The Del Medio fan, NW
1281 Argentina. *Journal of Geophysical Research: Earth Surface* 121, 2424–2445.
1282 <https://doi.org/10.1002/2016JF003912>, 2016.

1283 Schildgen, T.F., Robinson, R.A.J., Savi, S., Phillips, W.M., Spencer, J.Q.G., Bookhagen, B., Scherler,
1284 D., Tofelde, S., Alonso, R.N., Kubik, P.W., Binnie, S.A., Strecker, M.R. Landscape response
1285 to late Pleistocene climate change in NW Argentina: Sediment flux modulated by basin
1286 geometry and connectivity. *Journal of Geophysical Research: Earth Surface* 121, 392–414.
1287 <https://doi.org/10.1002/2015JF003607>, 2016.

1288 Schwab, K., Schäfer, A. Sedimentation und Tektonik im mittleren Abschnitt des Río Toro in der
1289 Ostkordillere NW-Argentiens. *Geologische Rundschau*, 65, 175-194.
1290 <https://doi.org/10.1007/BF01808462>, 1976.

1291 Schwanghart, W., Scherler, D. Short Communication: TopoToolbox 2 – MATLAB-based software for
1292 topographic analysis and modeling in Earth surface sciences. *Earth Surface Dynamics* 2, 1–7.
1293 <https://doi.org/10.5194/esurf-2-1-2014>, 2014.

1294 Simpson, G., Castelltort, S. Model shows that rivers transmit high-frequency climate cycles to the
1295 sedimentary record. *Geology* 40, 1131–1134. <https://doi.org/10.1130/G33451.1>, 2012.

1296 Seagren, E.G., Schoenbohm, L.M. Drainage reorganization across the Puna Plateau margin (NW
1297 Argentina): Implications for the preservation of orogenic plateaus. *Journal of Geophysical*
1298 *Research: Earth Surface*, 126(8), p.e2021JF006147. <https://doi.org/10.1029/2021JF006147>,
1299 2021.

1300 Seagren, E.G., McMillan, M., Schoenbohm, L.M. Tectonic control on drainage evolution in broken
1301 forelands: Examples from NW Argentina. *Tectonics*, 41(1), p.e2020TC006536,
1302 <https://doi.org/10.1029/2020TC006536>, 2022.

1303 Spelz, R.M., Fletcher, J.M., Owen, L.A. and Caffee, M.W. Quaternary alluvial-fan development,
1304 climate and morphologic dating of fault scarps in Laguna Salada, Baja California,
1305 Mexico. *Geomorphology*, 102(3-4), 578-594.
1306 <https://doi.org/10.1016/j.geomorph.2008.06.001>, 2008.

1307 Steffen, D., Schlunegger, F., Preusser, F. Late Pleistocene fans and terraces in the Majes valley,
1308 southern Peru, and their relation to climatic variations. *International Journal of Earth*
1309 *Sciences*, 99, 1975-1989. <https://doi.org/10.1007/s00531-009-0489-2>, 2010.

1310 Sternai, P., Herman, F., Valla, P.G., Champagnac, J.D. Spatial and temporal variations of glacial erosion
1311 in the Rhône valley (Swiss Alps): Insights from numerical modeling. *Earth and Planetary*
1312 *Science Letters* 368, 119–131. <https://doi.org/10.1016/j.epsl.2013.02.039>, 2013.

1313 Stone, J.O. Air pressure and cosmogenic isotope production. *Journal of Geophysical Research: Solid*
1314 *Earth* 105, 23753–23759, 2000.

1315 Strecker, M.R., Alonso, R., Bookhagen, B., Carrapa, B., Coutand, I., Hain, M.P., Hilley, G.E.,
1316 Mortimer, E., Schoenbohm, L., Sobel, E.R., 2009. Does the topographic distribution of the
1317 central Andean Puna Plateau result from climatic or geodynamic processes? *Geology*, 37(7),
1318 643-646. <https://doi.org/10.1130/G25545A.1>, 2009.

1319 Streit, R.L., Burbank, D.W., Strecker, M.R., Alonso, R.N., Cottle, J.M., Kylander-Clark, A.R.C.
1320 Controls on intermontane basin filling, isolation and incision on the margin of the Puna Plateau,
1321 NW Argentina (~23°S). *Basin Research* 29, 131–155. <https://doi.org/10.1111/bre.12141>, 2017.

1322 Terrizzano, C.M., García Morabito, E., Christl, M., Likerman, J., Tobal, J., Yamin, M., Zech, R.
1323 Climatic and Tectonic forcing on alluvial fans in the Southern Central Andes. *Quaternary*
1324 *Science Reviews* 172, 131–141. <https://doi.org/10.1016/j.quascirev.2017.08.002>, 2017.

1325 Tobal, J.E., Morabito, E.G., Terrizzano, C.M., Zech, R., Colavitto, B., Struck, J., Christl, M., Ghiglione,
1326 M.C. Quaternary landscape evolution of Patagonia at the Chilean Triple Junction: Climate and
1327 tectonic forcings. *Quaternary Science Reviews*, 261, 106960.
1328 <https://doi.org/10.1016/j.quascirev.2021.106960>, 2021.

- 1329 Tofelde, S., Duesing, W., Schildgen, T.F., Wickert, A.D., Wittmann, H., Alonso, R.N., Strecker, M.
 1330 Effects of deep-seated versus shallow hillslope processes on cosmogenic ¹⁰Be concentrations
 1331 in fluvial sand and gravel. *Earth Surface Processes and Landforms* 43, 3086–3098.
 1332 <https://doi.org/10.1002/esp.4471>, 2018.
- 1333 Tofelde, S., Savi, S., Wickert, A.D., Bufe, A., Schildgen, T.F. Alluvial channel response to
 1334 environmental perturbations: Fill-terrace formation and sediment-signal disruption. *Earth
 1335 Surface Dynamics* 7, 609–631. <https://doi.org/10.5194/esurf-7-609-2019>, 2019.
- 1336 Tofelde, S., Schildgen, T.F., Savi, S., Pingel, H., Wickert, A.D., Bookhagen, B., Wittmann, H., Alonso,
 1337 R.N., Cottle, J., Strecker, M.R. 100 kyr fluvial cut-and-fill terrace cycles since the Middle
 1338 Pleistocene in the southern Central Andes, NW Argentina. *Earth and Planetary Science Letters*
 1339 473, 141–153. <https://doi.org/10.1016/j.epsl.2017.06.001>, 2017.
- 1340 Uppala, S.M., Källberg, P.W., Simmons, A.J., Andrae, U., Bechtold, V.D.C., Fiorino, M., Gibson, J.K.,
 1341 Haseler, J., Hernandez, A., Kelly, G.A., Li, X., Onogi, K., Saarinen, S., Sokka, N., Allan, R.P.,
 1342 Andersson, E., Arpe, K., Balmaseda, M.A., Beljaars, A.C.M., Berg, L. Van De, Bidlot, J.,
 1343 Bormann, N., Caires, S., Chevallier, F., Dethof, A., Dragosavac, M., Fisher, M., Fuentes, M.,
 1344 Hagemann, S., Hólm, E., Hoskins, B.J., Isaksen, I., Janssen, P.A.E.M., Jenne, R., McNally,
 1345 A.P., Mahfouf, J.-F., Morcrette, J.-J., Rayner, N.A., Saunders, R.W., Simon, P., Sterl, A.,
 1346 Trenberth, K.E., Untch, A., Vasiljevic, D., Viterbo, P., Woollen, J. The ERA-40 re-analysis.
 1347 *Quarterly Journal of the Royal Meteorological Society* 131, 2961–3012.
 1348 <https://doi.org/10.1256/qj.04.176>, 2005.
- 1349 Valla, P.G., Shuster, D.L., Van Der Beek, P.A. Significant increase in relief of the European Alps during
 1350 mid-Pleistocene glaciations. *Nature Geoscience*, 4(10), 688-692.
 1351 <https://doi.org/10.1038/ngeo1242>, 2011.
- 1352 van den Berg, van Saproa, A.-P. H., Postma, G. Control of climate change on the yield of river
 1353 systems, Recent Adv. Model. Siliciclastic Shallow-Marine Stratigr. SEPM Spec. Publ., 90, 15–
 1354 33, 2008, <https://doi.org/10.2110/pec.08.90.0015>
- 1355 Ventra, D., Nichols, G.J. Autogenic dynamics of alluvial fans in endorheic basins: outcrop examples
 1356 and stratigraphic significance. *Sedimentology*, 61(3), 767-791.
 1357 <https://doi.org/10.1111/sed.12077>, 2014.
- 1358 Vera, C., Higgins, W., Amador, J., Ambrizzi, T., Garreaud, R., Gochis, D., Gutzler, D., Lettenmaier,
 1359 D., Marengo, J., Mechoso, C.R., Noguez-Paegle, J. Toward a unified view of the American
 1360 monsoon systems. *Journal of Climate*, 19(20), 4977-5000. <https://doi.org/10.1175/JCLI3896.1>,
 1361 2006.
- 1362 Vezzoli, L., Acocella, V., Omarini, R., Mazzuoli, R. Miocene sedimentation, volcanism and
 1363 deformation in the Eastern Cordillera (24°30' S, NW Argentina): Tracking the evolution of the
 1364 foreland basin of the Central Andes. *Basin Research* 24, 637–663.
 1365 <https://doi.org/10.1111/j.1365-2117.2012.00547.x>, 2012.
- 1366 Vizey, E.K., Cook, K.H. Relationship between Amazon and high Andes rainfall. *Journal of Geophysical
 1367 Research: Atmospheres*, 112(D7). <https://doi.org/10.1029/2006JD007980>, 2007.
- 1368 von Blanckenburg, F., T. Hewawasam, and P. W. Kubik (2004), Cosmogenic nuclide evidence for
 1369 low weathering and denudation in the wet, tropical highlands of Sri Lanka, *Journal of
 1370 Geophysical Research-Earth Surface*, 109(F3), <https://doi.org/10.1029/2003jf000049>.
- 1371 Wang, X., Auler, A.S., Edwards, R.L., Cheng, H., Ito, E., Wang, Y., Kong, X., Solheid, M. Millennial-
 1372 scale precipitation changes in southern Brazil over the past 90,000 years. *Geophysical Research
 1373 Letters* 34 (23). <https://doi.org/10.1029/2007GL031149>, 2007.
- 1374 Wickert, A.D., Schildgen, T.F. Long-profile evolution of transport-limited gravel-bed rivers. *Earth
 1375 Surface Dynamics*, 7(1), 17-43. <https://doi.org/10.5194/esurf-7-17-2019>, 2019.
- 1376 Wittmann, H., Malusà, M.G., Resentini, A., Garzanti, E., Niedermann, S. The cosmogenic record of
 1377 mountain erosion transmitted across a foreland basin: Source-to-sink analysis of in situ ¹⁰Be,
 1378 ²⁶Al and ²¹Ne in sediment of the Po river catchment. *Earth and Planetary Science Letters* 452,
 1379 258–271. <https://doi.org/10.1016/j.epsl.2016.07.017>, 2016.
- 1380 Zech, J., Terrizzano, C.M., Garcia Morabito, E., Veit, H., Zech, R. Timing and extent of late Pleistocene
 1381 glaciation in the arid Central Andes of Argentina and Chile (22°-41°S). *CIG* 43(2):697-
 1382 718. <http://dx.doi.org/10.18172/cig.3235>, 2017.

Formatted: Font colour: Auto

Formatted: Indent: Left: 0 cm, Hanging: 1.27 cm

Deleted:

1384 Zondervan, J.R., Stokes, M., Boulton, S.J., Telfer, M.W., Mather, A.E. Rock strength and structural
1385 controls on fluvial erodibility: Implications for drainage divide mobility in a collisional
1386 mountain belt. *Earth and Planetary Science Letters*, 538, 116221.
1387 <https://doi.org/10.1016/j.epsl.2020.116221>, 2020.
1388